Published October 17, 2011

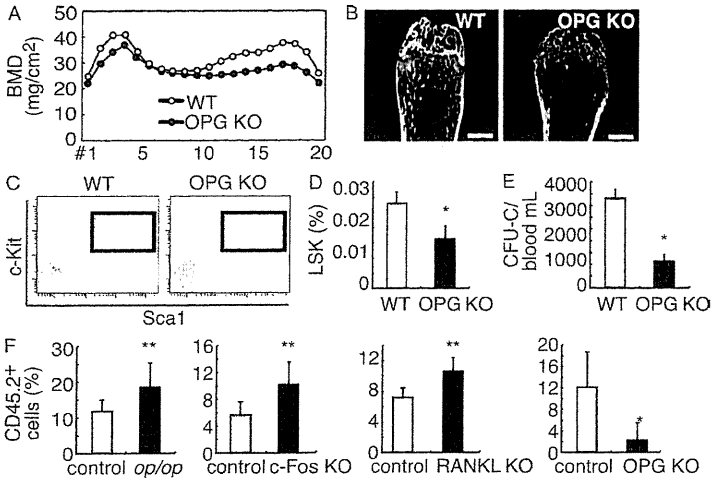

Figure 3. OPG-deficient mice are osteoporotic and have reduced HSPC pools. (A and B) BMD assays and microradiography analysis were undertaken in femurs of 8–12-wk-old OPG-deficient (OPG KO; $n = 5$) and wild-type (WT; $n = 5$) mice using dual-energy x-ray absorptiometry (mg/cm²; A) and micro-CT (B), respectively. BMD was shown in 20 longitudinal divisions of femurs. Bars, 1 mm. (C–E) 250 µg/kg/d G-CSF was injected subcutaneously into OPG-deficient (OPG KO; $n = 5$) and wild-type control (WT; $n = 5$) mice daily for 5 d. Peripheral blood was then collected, and the frequency of the LSK fraction (C and D) and CFU-C (E) were analyzed by flow cytometry and colony-forming assays, respectively. (C) Representative flow cytometry pattern of peripheral blood cells. Cells were gated with lineage-negative cells. Data represent the mean LSK frequency (%) ± SD in peripheral blood (*, $P < 0.01$, $n = 5$; D) and CFU-C ± SD in 1 ml peripheral blood (*, $P < 0.01$, $n = 12$; E). (F) 250 µg/kg/d G-CSF was injected subcutaneously into OPG-deficient (OPG KO), c-Fos–deficient (c-Fos KO), RANKL-deficient (RANKL KO), and littermate control mice daily for 5 d. Peripheral blood was collected from each mouse and transplanted into lethally irradiated Ly5.1 recipient mice with BM competitors isolated from Ly5.1 mice. Peripheral blood of recipient mice was collected after 3 mo of transplantation and stained with PE-conjugated anti-CD45.1 and FITC-conjugated anti-CD45.2, and leukocyte chimerism was determined by FACS. Data represent the mean CD45.2⁺ frequency (%) ± SD in peripheral blood (*, $P < 0.01$; **, $P < 0.05$, $n = 8$). Representative data of two (A, B, and F) and three (C, D, and E) independent experiments are shown.

HSPCs was observed in CD11b⁺ myeloid, B220⁺ B cell, and CD3⁺ T cell recipient lineages (Fig. S2). Thus, osteoclasts and BM cavities appear to antagonize HSC maintenance.

F4/80⁺ osteomacs are defective in *op/op* mice but appear normal in c-Fos– or OPG-deficient mice

Recently, it was reported that F4/80⁺ macrophages, termed osteomacs, reside in the endosteal (Chang et al., 2008) where they support osteoblast function, thereby contributing to retain HSCs in the BM niche (Winkler et al., 2010). Thus, increased HSPC mobilization seen in *op/op* mice after G-CSF injection could be a result of reduced levels of osteomacs. Indeed, we observed fewer F4/80⁺ osteomacs in *op/op* mice, although their levels in c-Fos–deficient and RANKL-deficient mice were similar to those observed in wild-type mice (Fig. 4). These observations suggest that osteomac reduction is not a common property of osteopetrotic mice, all of which show increased HSPC mobilization after G-CSF administration. CD11b⁺F4/80⁺Ly6-G⁺ macrophages, which also reportedly inhibit HSPC mobilization into the peripheral blood, are reduced after G-CSF treatment in wild-type mice (Winkler et al., 2010). However, like osteomacs, the CD11b⁺F4/80⁺Ly6-G⁺ macrophage population was reduced in *op/op* mice compared with wild-type mice, but such a reduction was not seen in c-Fos–deficient mice (Fig. S3 A). In OPG-deficient mice, osteomac and CD11b⁺F4/80⁺Ly6-G⁺ macrophage levels were similar to those seen in wild-type mice (Fig. 4 and Fig. S3 A). These results suggest that both of these cell types are M-CSF dependent and are deficient in the *op/op* model of osteopetrotic mice, but that this deficiency is not likely be the cause of increased mobilization of HSPCs seen in osteopetrotic animals. A more likely explanation is that HSPC mobilization seen in all osteopetrotic models is a result of loss of osteoclasts and BM cavities. Because F4/80⁺ osteomacs and CD11b⁺F4/80⁺Ly6-G⁺ macrophages were detected in osteoclast-deficient c-Fos–deficient mice, we do not consider F4/80⁺ cells to be osteoclasts. Indeed, F4/80 is reportedly not expressed in osteoclasts (Quinn et al., 1999).

The spleen is not the primary tissue that maintains HSPCs in *op/op* mice

Hematopoiesis in osteopetrotic mice reportedly occurs in extramedullary spaces, such as spleen (Lowell et al., 1996). Indeed, a greater proportion of LSK cells was seen in the

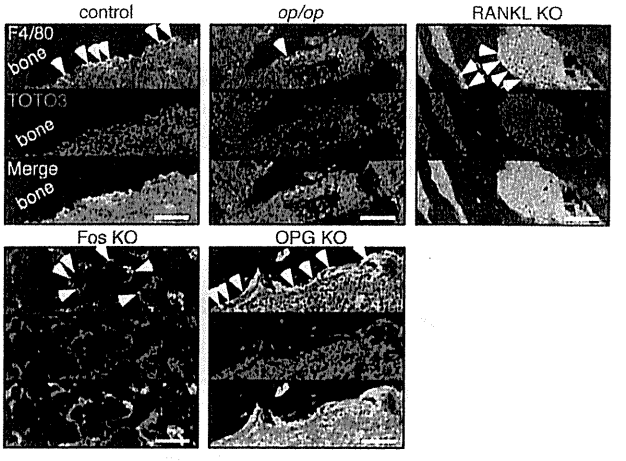

Figure 4. Osteomac levels are reduced in *op/op* but not c-Fos–deficient mice. Paraffin specimens of *op/op*, c-Fos–deficient (c-Fos KO), RANKL-deficient (RANKL KO), OPG-deficient (OPG KO), and control mouse femoral bones were stained with Alexa Fluor 488–conjugated anti-F4/80 antibody and observed under a confocal microscope. TOTO3 served as a nuclear stain. Arrowheads indicate F4/80-positive osteomacs. Representative data of three independent experiments are shown. Bars, 100 µm.

Published October 17, 2011

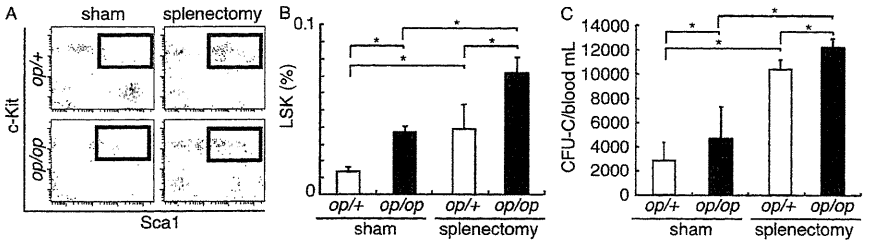

Figure 5. HSCs do not accumulate in the spleen of *op/op* mice. Splenectomy or sham surgery was performed on 8–12-wk-old *op/op* ($n = 5$ for each group) and control (*op/+*; $n = 5$ for each group) mice. 7 d later, mice were injected with 250 µg/kg/d G-CSF daily for 5 d, and mobilization of HSCs to peripheral blood was analyzed using flow cytometry and colony-forming assays. (A) Representative flow cytometry pattern of peripheral blood after G-CSF injection ($n = 5$ for each group). Cells were gated on lineage-negative cells. (B and C) Data represent the mean LSK frequency (%) ± SD in peripheral blood (*, $P < 0.01$, $n = 5$ for each group; B) and mean CFU-C ± SD in 1 ml peripheral blood (*, $P < 0.01$, $n = 5$ for each group; C). Representative data of three independent experiments are shown.

spleen of *op/op* mice than in control (*op/+*) mice (Fig. S3, B and C). Thus, we removed the spleen from *op/op* mice and treated those mice with G-CSF serially to analyze HSPC mobilization (Fig. 5). Interestingly, HSPC mobilization was induced or even significantly higher in splenectomized *op/op* mice compared with sham-operated *op/op* mice (Fig. 5). These data suggest that HSCs are maintained in tissues other than spleen in osteoclast-deficient osteopetrotic mice. Interestingly, we found that bone tissues in osteoclast-deficient mice contained small spaces where c-Kit–positive hematopoietic cells are located (Fig. S4 A). Thus, hematopoiesis may be maintained in bone, even in osteopetrotic mice. In fact, flow cytometry analysis revealed an HSC-enriched LSK population in osteopetrotic bones of *op/op* mice (Fig. S4 B), and these cells were shown to be functional by an LTC-IC assay (not depicted). These results indicate that HSCs are maintained in bones of osteopetrotic mice, that increased bone mass as a result of impaired osteoclastogenesis may increase functionality of the HSC niche, and that osteoclasts could be a therapeutic target to expand HSCs as well as bone mass. Bones are formed by osteoblasts, and osteoblasts reportedly express various niche factors such as angiopoietin 1, osteopontin, Cxcl12, and KitL (Arai et al., 2004; Stier et al., 2005; Adams and Scadden, 2006; Katayama et al., 2006). We found that these niche factors were expressed in osteopetrotic bones of *op/op*, c-Fos–deficient, and RANKL-deficient mice (unpublished data).

Osteoclast-inhibiting agents increase HSPC mobilization in wild-type mice

Finally, we asked whether blocking osteoclast function or differentiation pharmacologically would inhibit or enhance hematopoietic activity in wild-type mice. Wild-type mice were pretreated with bisphosphonate (alendronate) or vehicle (PBS), and HSPC mobilization after serial G-CSF injection was analyzed (Fig. 6). Bisphosphonate treatment significantly increased bone mass (Fig. 6, A and B), and, interestingly, mobilization of HSPCs as determined by a colony-forming assay was highly induced in bisphosphonate- compared with vehicle-treated mice (Fig. 6 C). Thus, bisphosphonate therapy increased bone mass and up-regulated HSPC mobilization. Similar phenotypes were detected in mice treated with neutralizing RANKL antibody compared with isotype-matched control antibody-treated mice (Fig. 6, D–F). Thus our results demonstrate that HSCs can be expanded pharmacologically. Treatment with zoledronate, another bisphosphonate, also reportedly increased HSPC mobilization in response to G-CSF (Winkler et al., 2010), further suggesting that bisphosphonate, neutralizing RANKL antibody, or other osteoclast inhibitors might serve as adjuvants to increase HSPC mobilization.

Collectively, our results challenge the dogma that BM cavity–deficient animals cannot maintain HSCs and raises the question of why mammalian and avian species developed BM cavities. Although the density of osteopetrotic bones in *op/op* mice was greater than that seen in controls (Fig. S5 A), strength

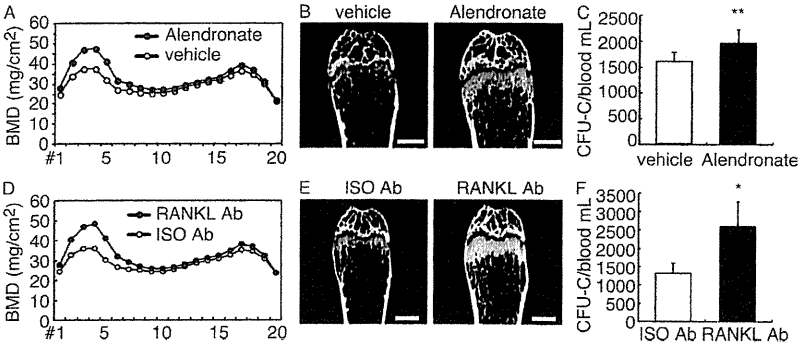

Figure 6. Pharmacological inhibition of osteoclasts increases bone mass and expands the HSC pool in wild-type mice. (A–C) Wild-type mice were treated with 5 mg per mouse of alendronate (bisphosphonate; $n = 5$) or vehicle (PBS; $n = 5$) daily for 14 d and then injected with 250 µg/kg/d G-CSF daily for five more days. Mice were assessed for BMD (A), microradiography (B), and HSC mobilization in peripheral blood (C; **, $P < 0.05$, $n = 5$). Bar, 1 mm. (D and E) Wild-type mice were treated with 5 or 2.5 mg/kg of neutralizing antibody against RANKL (RANKL Ab; $n = 5$) or isotype control antibody (ISO; $n = 5$) 14 and 1 d before G-CSF injection, respectively. Mice were then injected with 250 µg/kg/d G-CSF daily for 5 d, and BMD (D), microradiography (E), and mobilization of HSCs in peripheral blood (F; *, $P < 0.01$, $n = 5$) were analyzed. BMD was shown in 20 longitudinal divisions of femurs (A and D). Data represent mean CFU-C ± SD in 1 ml peripheral blood (C and F). Bars, 1 mm. Representative data of two independent experiments are shown.

Published October 17, 2011

tests indicated that bones were more fragile than control bones (Fig. S5 B). Fractures were induced in osteopetrotic bones earlier and by lower energy than in control bones, based on constant displacement tests (Fig. S5, B and C). Osteopetrotic bone also showed reduced elasticity (Fig. S5 D). H/E staining indicated that *op/op* mouse bones were filled with trabecular bone and that mutants exhibited thinner cortical bones than did control mice (Fig. S5, E and F). Indeed, osteopetrotic patients suffer from frequent fractures (Landa et al., 2007). Thus bones likely developed not only to maintain HSCs but to optimize bone strength and body support. To overcome the reduced ability to support HSCs in an open BM cavity created by osteoclasts, BM niches were likely developed by osteoblastic cells, vascular endothelial cells, reticular cells, or aggregates of these cells (Adams and Scadden, 2006; Kiel and Morrison, 2008), or by the products of these cells such as angiopoietin 1, osteopontin, Cxcl12, and thrombopoietin 1 (Calvi et al., 2003; Zhang et al., 2003; Arai et al., 2004; Kiel et al., 2005; Stier et al., 2005; Adams and Scadden, 2006; Sugiyama et al., 2006; Kiel and Morrison, 2008; Lymperi et al., 2010).

Manipulating HSCs in vitro to increase their number likely results in reduced stemness because quiescence is essential to maintain stem cell function (Cheng et al., 2000; Miyamoto et al., 2007). Thus, there is likely an antagonistic relationship between expansion and quiescence in HSC expansion. Bone mineral density (BMD) decreases with age, as osteoporosis is increased by osteoclastic activity (Manolagas and Jilka, 1995; Teitelbaum, 2007). Hematopoietic activity also decreases with age (Geiger and Rudolph, 2009; Waterstrat and Van Zant, 2009), suggesting that bone aging can cause both reduced bone mass and reduced hematopoiesis, and that antagonizing osteoclasts pharmacologically could promote increased bone mass and stimulate an induced niche in vivo to increase the HSC pool.

MATERIALS AND METHODS

Mice. *op/op*, c-Fos–deficient, and RANKL-deficient mice were generated by crossing heterozygotes of respective genotypes. c-Fos-deficient mice were provided by E. Wagner (Institute of Molecular Biotechnology of the Austrian Academy of Sciences, Vienna, Austria). Animals were maintained under pathogen-free conditions in animal facilities certified by the Keio University School of Medicine animal care committee. To analyze blood counts, peripheral blood from the postorbital vein was collected in heparinized microtubes (Drummond Scientific). 5-FU (Kyowa Hakko Kirinn) was administered intravenously at 150 mg/kg to 8–12-wk-old *op/op*, c-Fos–deficient, or littermate control mice once a week, and mouse survival was monitored daily. Animal protocols were approved by the Keio University School of Medicine animal care committee.

Analysis of skeletal morphology. 8–12-wk-old mice were necropsied, and their hindlimbs were removed, fixed in 70% ethanol, and subjected to dual energy x-ray absorptiometry analysis to measure BMD and for microradiographic analysis. BMD was shown in 20 longitudinal divisions of femurs.

Mobilization of hematopoietic progenitors. To induce HSPC mobilization, mice were injected with recombinant human G-CSF (Kyowa Hakko Kirin Co.; 250 μg/kg/d for 5 d, subcutaneous injection). Peripheral blood was harvested 3 h after the last G-CSF injection and used for blood counts, determination of colony-forming units in culture (CFU-C), and flow cytometric (FACS) analysis. Blood counts were analyzed using CellTac (Nihon Kohden). For CFU-C assays, cells were cultured in methylcellulose medium containing recombinant mouse (rm) stem cell factor, rm IL-3, recombinant human (rh) IL-6, and rh erythropoietin (MethoCult GF M3434; STEMCELL Technologies) in 35-mm culture dishes (Falcon) and incubated at 37°C in 5% CO_2. The number of CFU-Cs was determined on day 7 using a microscope (Olympus). FACS analysis was undertaken as described. For some experiments, Alendronate or RANKL neutralizing antibody was administered. 5 μg alendronate/mouse/d was injected subcutaneously for 14 d before G-CSF injection. 5 mg/kg RANKL neutralizing antibody (Oriental Yeast Co.) or isotype control antibody (BD) at 14 d and 2.5 mg/kg at 1 d before G-CSF injection was injected into the peritoneal cavity. For competitive repopulation assays, peripheral blood from individual CD45.2$^+$ mice was pooled, and 20 μl of pooled blood was mixed with 500,000 competitive BM cells from untreated CD45.1$^+$ mice and injected intravenously into lethally irradiated CD45.1$^+$ recipient mice. After 3 mo of transplantation, peripheral blood reconstitution in multiple lineages was determined by FACS using CD45.1 (A20), CD45.2 (104), Mac1 (M1/70), CD3 (500A2), and B220 (RA3-6B2) antibodies (all BD).

Flow cytometry. mAbs (all BD) recognizing the following markers were used for flow cytometric analyses and cell sorting: c-Kit (2B8), Sca-1 (E13-161.7), CD3 (500A2) B220 (RA3-6B2), TER-119 (Ly-76), Gr-1 (RB6-8C5), and Mac-1 (M1/70). A mixture of mAbs recognizing CD3, B220, TER-119, Mac-1, or Gr-1 was used to identify lineage$^+$ cells. Mature myeloid cells were stained with PEcy7-conjugated anti-CD11b (M1/70; eBioscience), Alexa Fluor 488–conjugated anti-F4/80 (CI:A3-1; BioLegend), and PE-conjugated anti–Ly6-G antibody (1A8; BD). Stained cells were analyzed on a FACS Aria2 machine (BD).

ELISA. Serum M-CSF levels were assayed using the Mouse M-CSF ELISA kit (R&D Systems), according to the manufacturer's instructions.

Immunohistochemical analysis. Frozen sections of *op/op* mice femoral bone that had not been decalcified were stained with goat anti–c-Kit antibody (AF1356; R&D Systems), followed by Alexa Fluor 488–conjugated donkey anti–goat antibody (Invitrogen) to detect HSCs and with TOTO3 (Invitrogen) to detect nuclei. Samples were observed under a fluorescence microscope (IX70; Olympus). Paraffin sections of wild-type, *op/op*, c-Fos–deficient, and OPG–deficient mice femoral bone were stained with Alexa Fluor 488–conjugated anti-F4/80 antibody (BioLegend) and TOTO3 as a nuclear stain and then observed under a confocal microscope (FV1000; Olympus).

Bone strength test. The femur was removed from mice and placed on the lower supports of a three point bending fixture with the anterior side facing up using an apparatus called the Bone Strength Tester MZ-500S (Maruto) installed with a load of 50 N. The span between the two lower supports was set at 6 mm. For all femoral specimens, the upper loading device was aligned to the center of the femoral shaft and the load was applied at a constant displacement rate of 10 mm/min until breakage occurred.

Online supplemental material. Fig. S1 demonstrates the sensitivity of c-Fos–deficient and *op/op* mice to 5-FU, and the bone phenotype of RANKL-deficient mice. Fig. S2 shows multilineage reconstitution of donor-derived cells in recipient mice. Fig. S3 demonstrates the frequency of the CD11b$^+$F4/80$^+$Ly6-G$^+$ macrophage population in wild-type, *op/op*, c-Fos–deficient, and OPG-deficient mice, and the frequency of LSK cells in *op/op* mouse spleen. Fig. S4 demonstrates the presence of HSCs in osteopetrotic bone. Fig. S5 shows osteopetrotic bone strength. Online supplemental material is available at http://www.jem.org/cgi/content/full/jem.20101890/DC1.

We thank Professor Wagner for providing c-Fos–deficient mice and Drs. Momoshima, Ishikawa, and Mogoe, Mr. Yamazaki, and Mrs. K. Fukushima for technical support.

K. Miyamoto was supported by a grant-in-aid for Young Scientists (B). T. Miyamoto was supported by a grant-in-aid for Young Scientists (A) and by Precursory Research for Embryonic Science and Technology (PREST), the Takeda Science Foundation, the Nakatomi Foundation, the Inamori Foundation, and the Keio Kanrinmaru project, Japan.

The authors have no conflicting financial interests.

Submitted: 9 September 2010
Accepted: 22 September 2011

Published October 17, 2011

REFERENCES

Adams, G.B., and D.T. Scadden. 2006. The hematopoietic stem cell in its place. *Nat. Immunol.* 7:333–337 . http://dx.doi.org/10.1038/ni1331

Arai, F., A. Hirao, M. Ohmura, H. Sato, S. Matsuoka, K. Takubo, K. Ito, G.Y. Koh, and T. Suda. 2004. Tie2/angiopoietin-1 signaling regulates hematopoietic stem cell quiescence in the bone marrow niche. *Cell.* 118: 149–161. http://dx.doi.org/10.1016/j.cell.2004.07.004

Bucay, N., I. Sarosi, C.R. Dunstan, S. Morony, J. Tarpley, C. Capparelli, S. Scully, H.L. Tan, W. Xu, D.L. Lacey, et al. 1998. osteoprotegerin-deficient mice develop early onset osteoporosis and arterial calcification. *Genes Dev.* 12:1260–1268. http://dx.doi.org/10.1101/gad.12.9.1260

Calvi, L.M., G.B. Adams, K.W. Weibrecht, J.M. Weber, D.P. Olson, M.C. Knight, R.P. Martin, E. Schipani, P. Divieti, F.R. Bringhurst, et al. 2003. Osteoblastic cells regulate the haematopoietic stem cell niche. *Nature.* 425:841–846. http://dx.doi.org/10.1038/nature02040

Chang, M.K., L.J. Raggatt, K.A. Alexander, J.S. Kuliwaba, N.L. Fazzalari, K. Schroder, E.R. Maylin, V.M. Ripoll, D.A. Hume, and A.R. Pettit. 2008. Osteal tissue macrophages are intercalated throughout human and mouse bone lining tissues and regulate osteoblast function in vitro and in vivo. *J. Immunol.* 181:1232–1244.

Cheng, T., N. Rodrigues, H. Shen, Y. Yang, D. Dombkowski, M. Sykes, and D.T. Scadden. 2000. Hematopoietic stem cell quiescence maintained by p21cip1/waf1. *Science.* 287:1804–1808. http://dx.doi.org/10.1126/science.287.5459.1804

Chitu, V., and E.R. Stanley. 2006. Colony-stimulating factor-1 in immunity and inflammation. *Curr. Opin. Immunol.* 18:39–48. http://dx.doi.org/10.1016/j.coi.2005.11.006

Christopher, M.J., and D.C. Link. 2008. Granulocyte colony-stimulating factor induces osteoblast apoptosis and inhibits osteoblast differentiation. *J. Bone Miner. Res.* 23:1765–1774. http://dx.doi.org/10.1359/jbmr.080612

Freedman, M.H., and E.F. Saunders. 1981. Hematopoiesis in the human spleen. *Am. J. Hematol.* 11:271–275. http://dx.doi.org/10.1002/ajh.2830110307

Geiger, H., and K.L. Rudolph. 2009. Aging in the lympho-hematopoietic stem cell compartment. *Trends Immunol.* 30:360–365. http://dx.doi.org/10.1016/j.it.2009.03.010

Grigoriadis, A.E., Z.Q. Wang, M.G. Cecchini, W. Hofstetter, R. Felix, H.A. Fleisch, and E.F. Wagner. 1994. c-Fos: a key regulator of osteoclast-macrophage lineage determination and bone remodeling. *Science.* 266: 443–448. http://dx.doi.org/10.1126/science.7939685

Heissig, B., K. Hattori, S. Dias, M. Friedrich, B. Ferris, N.R. Hackett, R.G. Crystal, P. Besmer, D. Lyden, M.A. Moore, et al. 2002. Recruitment of stem and progenitor cells from the bone marrow niche requires MMP-9 mediated release of kit-ligand. *Cell.* 109:625–637. http://dx.doi.org/10.1016/S0092-8674(02)00754-7

Katayama, Y., M. Battista, W.M. Kao, A. Hidalgo, A.J. Peired, S.A. Thomas, and P.S. Frenette. 2006. Signals from the sympathetic nervous system regulate hematopoietic stem cell egress from bone marrow. *Cell.* 124:407–421. http://dx.doi.org/10.1016/j.cell.2005.10.041

Kiel, M.J., and S.J. Morrison. 2008. Uncertainty in the niches that maintain haematopoietic stem cells. *Nat. Rev. Immunol.* 8:290–301. http://dx.doi.org/10.1038/nri2279

Kiel, M.J., O.H. Yilmaz, T. Iwashita, O.H. Yilmaz, C. Terhorst, and S.J. Morrison. 2005. SLAM family receptors distinguish hematopoietic stem and progenitor cells and reveal endothelial niches for stem cells. *Cell.* 121: 1109–1121. http://dx.doi.org/10.1016/j.cell.2005.05.026

Kollet, O., A. Dar, S. Shivtiel, A. Kalinkovich, K. Lapid, Y. Sztainberg, M. Tesio, R.M. Samstein, P. Goichberg, A. Spiegel, et al. 2006. Osteoclasts degrade endosteal components and promote mobilization of hematopoietic progenitor cells. *Nat. Med.* 12:657–664. http://dx.doi.org/10.1038/nm1417

Kong, Y.Y., H. Yoshida, I. Sarosi, H.L. Tan, E. Timms, C. Capparelli, S. Morony, A.J. Oliveira-dos-Santos, G. Van, A. Itie, et al. 1999. OPGL is a key regulator of osteoclastogenesis, lymphocyte development and lymph-node organogenesis. *Nature.* 397:315–323. http://dx.doi.org/10.1038/16852

Landa, J., N. Margolis, and P. Di Cesare. 2007. Orthopaedic management of the patient with osteopetrosis. *J. Am. Acad. Orthop. Surg.* 15:654–662.

Lowell, C.A., M. Niwa, P. Soriano, and H.E. Varmus. 1996. Deficiency of the Hck and Src tyrosine kinases results in extreme levels of extramedullary hematopoiesis. *Blood.* 87:1780–1792.

Lymperi, S., F. Ferraro, and D.T. Scadden. 2010. The HSC niche concept has turned 31. Has our knowledge matured? *Ann. N. Y. Acad. Sci.* 1192:12–18. http://dx.doi.org/10.1111/j.1749-6632.2009.05223.x

Manolagas, S.C., and R.L. Jilka. 1995. Bone marrow, cytokines, and bone remodeling. Emerging insights into the pathophysiology of osteoporosis. *N. Engl. J. Med.* 332:305–311. http://dx.doi.org/10.1056/NEJM199502023320506

Miyamoto, K., K.Y. Araki, K. Naka, F. Arai, K. Takubo, S. Yamazaki, S. Matsuoka, T. Miyamoto, K. Ito, M. Ohmura, et al. 2007. Foxo3a is essential for maintenance of the hematopoietic stem cell pool. *Cell Stem Cell.* 1:101–112. http://dx.doi.org/10.1016/j.stem.2007.02.001

Miyamoto, T., O. Ohneda, F. Arai, K. Iwamoto, S. Okada, K. Takagi, D.M. Anderson, and T. Suda. 2001. Bifurcation of osteoclasts and dendritic cells from common progenitors. *Blood.* 98:2544–2554. http://dx.doi.org/10.1182/blood.V98.8.2544

Mizuno, A., N. Amizuka, K. Irie, A. Murakami, N. Fujise, T. Kanno, Y. Sato, N. Nakagawa, H. Yasuda, S. Mochizuki, et al. 1998. Severe osteoporosis in mice lacking osteoclastogenesis inhibitory factor/osteoprotegerin. *Biochem. Biophys. Res. Commun.* 247:610–615. http://dx.doi.org/10.1006/bbrc.1998.8697

Quinn, J.M., M. Morfis, M.H. Lam, J. Elliott, V. Kartsogiannis, E.D. Williams, M.T. Gillespie, T.J. Martin, and P.M. Sexton. 1999. Calcitonin receptor antibodies in the identification of osteoclasts. *Bone.* 25:1–8. http://dx.doi.org/10.1016/S8756-3282(99)00094-0

Stier, S., Y. Ko, R. Forkert, C. Lutz, T. Neuhaus, E. Grünewald, T. Cheng, D. Dombkowski, L.M. Calvi, S.R. Rittling, and D.T. Scadden. 2005. Osteopontin is a hematopoietic stem cell niche component that negatively regulates stem cell pool size. *J. Exp. Med.* 201:1781–1791. http://dx.doi.org/10.1084/jem.20041992

Sugiyama, T., H. Kohara, M. Noda, and T. Nagasawa. 2006. Maintenance of the hematopoietic stem cell pool by CXCL12-CXCR4 chemokine signaling in bone marrow stromal cell niches. *Immunity.* 25:977–988. http://dx.doi.org/10.1016/j.immuni.2006.10.016

Takamatsu, Y., P.J. Simmons, R.J. Moore, H.A. Morris, L.B. To, and J.P. Lévesque. 1998. Osteoclast-mediated bone resorption is stimulated during short-term administration of granulocyte colony-stimulating factor but is not responsible for hematopoietic progenitor cell mobilization. *Blood.* 92:3465–3473.

Teitelbaum, S.L. 2007. Osteoclasts: what do they do and how do they do it? *Am. J. Pathol.* 170:427–435. http://dx.doi.org/10.2353/ajpath.2007.060834

Watanabe, T., H. Suzuya, T. Onishi, S. Kanai, M. Kaneko, H. Watanabe, R. Nakagawa, Y. Kawano, Y. Takaue, Y. Kuroda, and J.E. Talmadge. 2003. Effect of granulocyte colony-stimulating factor on bone metabolism during peripheral blood stem cell mobilization. *Int. J. Hematol.* 77:75–81. http://dx.doi.org/10.1007/BF02982606

Waterstrat, A., and G. Van Zant. 2009. Effects of aging on hematopoietic stem and progenitor cells. *Curr. Opin. Immunol.* 21:408–413. http://dx.doi.org/10.1016/j.coi.2009.05.002

Winkler, I.G., N.A. Sims, A.R. Pettit, V. Barbier, B. Nowlan, F. Helwani, I.J. Poulton, N. van Rooijen, K.A. Alexander, L.J. Raggatt, and J.P. Lévesque. 2010. Bone marrow macrophages maintain hematopoietic stem cell (HSC) niches and their depletion mobilizes HSCs. *Blood.* 116: 4815–4828. http://dx.doi.org/10.1182/blood-2009-11-253534

Yoshida, H., S. Hayashi, T. Kunisada, M. Ogawa, S. Nishikawa, H. Okamura, T. Sudo, L.D. Shultz, and S. Nishikawa. 1990. The murine mutation osteopetrosis is in the coding region of the macrophage colony stimulating factor gene. *Nature.* 345:442–444. http://dx.doi.org/10.1038/345442a0

Zhang, J., C. Niu, L. Ye, H. Huang, X. He, W.G. Tong, J. Ross, J. Haug, T. Johnson, J.Q. Feng, et al. 2003. Identification of the haematopoietic stem cell niche and control of the niche size. *Nature.* 425:836–841. http://dx.doi.org/10.1038/nature02041

Dual functions of cell-autonomous and non–cell-autonomous ADAM10 activity in granulopoiesis

Masaki Yoda,[1,2] Tokuhiro Kimura,[3] Takahide Tohmonda,[1,2] Shinichi Uchikawa,[2] Takeshi Koba,[2] Jiro Takito,[1,2] Hideo Morioka,[2] Morio Matsumoto,[2] Daniel C. Link,[4] Kazuhiro Chiba,[2] Yasunori Okada,[3] Yoshiaki Toyama,[2] and Keisuke Horiuchi[1,2]

Departments of [1]Anti-Aging Orthopedic Research, [2]Orthopedic Surgery, and [3]Pathology, School of Medicine, Keio University, Tokyo, Japan; and [4]Department of Medicine, Washington University, St Louis, MO

Previous studies have revealed various extrinsic stimuli and factors involved in the regulation of hematopoiesis. Among these, Notch-mediated signaling has been suggested to be critically involved in this process. Herein, we show that conditional inactivation of ADAM10, a membrane-bound protease with a crucial role in Notch signaling (S2 cleavage), results in myeloproliferative disorder (MPD) highlighted by severe splenomegaly and increased populations of myeloid cells and hematopoietic stem cells. Reciprocal transfer of bone marrow cells between wild-type and ADAM10 mutant mice revealed that ADAM10 activity in both hematopoietic and nonhematopoietic cells is involved in the development of MPD. Notably, we found that MPD caused by lack of ADAM10 in nonhematopoietic cells was mediated by G-CSF, whereas MPD caused by ADAM10-deficient hematopoietic cells was not. Taken together, the present findings reveal previously undescribed nonredundant roles of cell-autonomous and non–cell-autonomous ADAM10 activity in the maintenance of hematopoiesis. (*Blood*. 2011;118(26):6939-6942)

Introduction

Notch signaling plays crucial roles in cell fate decision in diverse tissues.[1] Previous studies have shown the potential involvement of Notch receptors and their ligands in the maintenance of hematopoietic stem cells (HSCs) in bone marrow (BM).[2,3] However, despite intensive studies in the past decade, the physiologic relevance of Notch signaling in HSC maintenance remains controversial. Gain-of-function experiments both in vitro and in vivo suggest that Notch signaling in HSCs increases self-renewal and suppresses differentiation of HSCs.[4-7] Conversely, others have shown that Notch signaling in HSCs is dispensable for their maintenance.[8,9]

The metalloprotease responsible for S2 cleavage of Notch also remains controversial. Initial studies identified ADAM17/TACE, a membrane-bound metalloprotease belonging to the ADAM gene family, as the sheddase for Notch.[10] However, findings that *Adam17* mutant mice did not exhibit any Notch-related developmental defects raised questions about the relevance of ADAM17 for Notch processing in vivo.[11,12] On the other hand, emerging evidence suggests that another family member, ADAM10, is the major protease responsible for Notch processing.[13-16]

To clarify these issues, we generated conditional ADAM10-deficient mice and found that conditional inactivation of ADAM10 by the inducible *Mx1-Cre* transgene results in myeloproliferative disorder (MPD), which resembles that observed in Notch signaling–defective mutant mice.[17-20] Reciprocal BM transplantation experiments revealed that lack of ADAM10 in either hematopoietic cells or the host environment leads to the MPD phenotype. Furthermore, we found that MPD caused by lack of ADAM10 in the host environment, but not in hematopoietic cells, is dependent on G-CSF. Thus, the present study reveals previously undescribed nonredundant roles of cell-autonomous and non–cell-autonomous ADAM10 activity in the regulation of hematopoiesis.

Methods

A detailed description of the gene targeting and generation of *Adam10*$^{flox/flox}$ mice is provided in supplemental Methods (available on the *Blood* Web site; see the Supplemental Materials link at the top of the online article). *Adam10*$^{flox/flox}$ mice exhibited no apparent defects (data not shown) and were used as control animals for the experiments (henceforth referred to as control mice). *Adam10*$^{flox/flox}$ mice were crossed with *Mx1-Cre* transgenic mice[21] to generate inducible conditional ADAM10-knockout mice (*Adam10*$^{flox/flox}$/*Mx1-Cre*$^{+}$, henceforth referred to as *Adam10/Mx1* mice). Conditional excision of the floxed allele was achieved by intraperitoneal injection of polyinosinic:polycytidylic acid. All animal experiments were approved by the Institutional Animal Care and Use Committee of the Keio University School of Medicine. All other experimental methods are described in supplemental Methods.

Images of the sections were acquired with ACT-1 Version 2.62 software (Nikon) via a digital camera (DXM1200; Nikon) mounted on a BX50 microscope (Olympus). The objectives used were 4×/0.16, 10×/0.40, and 20×/0.70 UPlanApo (Olympus). Images were processed with Adobe Photoshop CS4 (Adobe Systems).

Results and discussion

Conditional inactivation of ADAM10 results in MPD

To elucidate the roles of ADAM10 in hematopoiesis and its potential involvement in Notch signaling, we generated a mutant

Submitted June 2, 2011; accepted October 21, 2011. Prepublished online as *Blood* First Edition paper, October 31, 2011; DOI 10.1182/blood-2011-06-357210.

The online version of this article contains a data supplement.

The publication costs of this article were defrayed in part by page charge payment. Therefore, and solely to indicate this fact, this article is hereby marked "advertisement" in accordance with 18 USC section 1734.

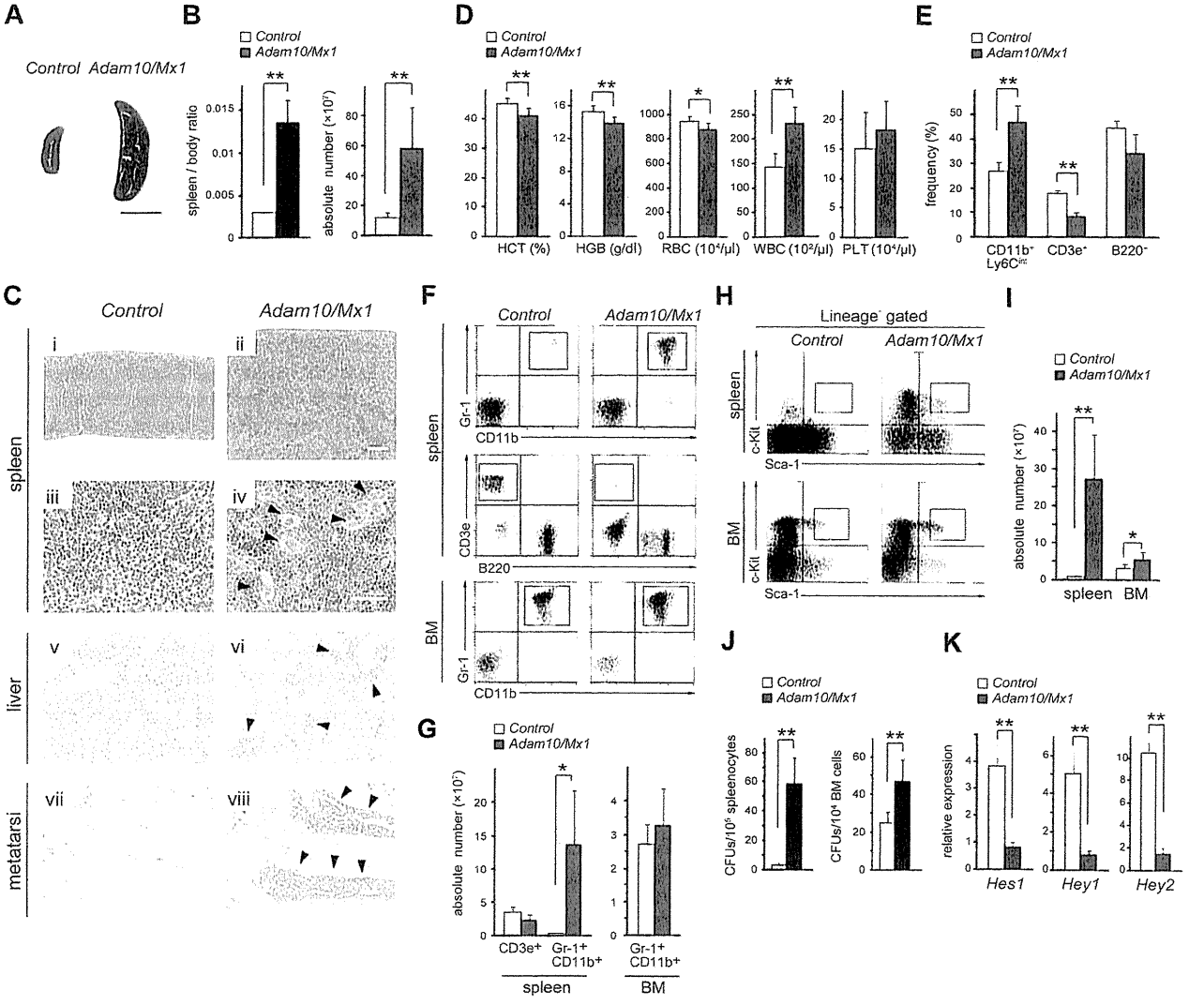

Figure 1. Conditional inactivation of ADAM10 results in MPD. (A) Gross morphology of spleen from 8-week-old control and *Adam10/Mx1* mice injected with polyinosinic:polycytidylic acid at 4 weeks before euthanasia (scale bar represents 1 cm). (B) Spleen/body weight ratios and total cell counts in the spleen. Bars indicate mean ± SD (n = 5). (C) H&E staining of sections of the spleen (i-iv; bars represent 200 μm [i and ii] and 50 μm [iii and iv]), liver (v and vi; bar represents 100 μm), and metatarsi (vii and viii; bar represents 250 μm) from 12-week-old control and *Adam10/Mx1* mice injected with polyinosinic:polycytidylic acid at 8 weeks before euthanasia. The spleen of *Adam10/Mx1* mice shows an increase in the number of myeloid cells, as well as megakaryocytes (arrowheads) in the red pulp (i-iv). In addition, granulocytic cells are present in the liver of *Adam10/Mx1* mice, which indicates extramedullary hematopoiesis (v and vi arrowheads). The metatarsi of the mutant mice are filled with hematopoietic cells, whereas the BM cavity of control animals is filled with adipose cells (vii and viii arrowheads). (D) Complete blood counts for control and *Adam10/Mx1* mice. Bars indicate mean ± SD (n = 4); HCT, hematocrit; HGB, hemoglobin; RBC, red blood cells; WBC, white blood cells; and PLT, platelets. (E) Flow cytometric analysis of peripheral blood. Bars indicate mean ± SD (n = 4). (F) Flow cytometric analysis of $CD3e^+$, and $B220^+$ cells in the spleen and $Gr\text{-}1^+$ $CD11b^+$ cells in the BM from control and *Adam10/Mx1* mice (boxed areas). (G) Absolute cell numbers of $Gr\text{-}1^+$ $CD11b^+$ cells in the BM and $CD3e^+$ and $Gr\text{-}1^+$ $CD11b^+$ cells in the spleen. Bars indicate mean ± SD (n = 4). (H) Flow cytometric analysis of the KSL cell populations in the BM and spleen of control and *Adam10/Mx1* mice. Boxed areas indicate KSL cells. (I) Absolute numbers of KSL cells in the BM and spleen. Bars indicate mean ± SD (n = 3). (J) Numbers of colony-forming units (CFUs) per 1×10^5 splenocytes and 1×10^4 BM cells, respectively. Bars indicate mean ± SD (n = 5). The flow cytometric analysis shown here is a representative result of 3 independent experiments. (K) Transcript levels of *Hes1*, *Hey1*, and *Hey2* in the spleen of control and *Adam10/Mx1* mice. *t* test: $^*P < .05$, $^{**}P < .005$.

line (*Adam10/Mx1*) in which temporal and systemic deletion of *Adam10* was achieved by the *Mx1-Cre* transgene.[21] Notably, *Adam10/Mx1* mice developed severe splenomegaly characterized by expansion of the red pulp (Figure 1A-B, Ci-iv). Infiltration of myeloid cells was also observed in the liver of *Adam10/Mx1* mice (Figure 1Cv-vi). The metatarsal BM, which is usually replaced by fat cells in adult mice, was filled with hematopoietic cells (Figure 1Cvii-viii). The complete blood counts revealed decreases in hemoglobulin and hematocrit and an increase in the number of white blood cells (Figure 1D). Flow cytometric analysis of peripheral blood cells showed a relative increase in neutrophils ($CD11b^+$ $Ly6C^{int}$), as well as a decrease in a T-cell population ($CD3e^+$; Figure 1E).

Flow cytometric analysis of splenocytes from *Adam10/Mx1* mice revealed an increase in the population of $Gr\text{-}1^+CD11b^+$ myeloid cells (Figure 1F-G), whereas no significant difference was observed in the BM of the femur. There was also a significant increase in HSCs ($c\text{-}Kit^+Sca\text{-}1^+Lin^-$; KSL cells[22]) in *Adam10/Mx1* mice (Figure 1H-I). Consistent with these findings, there were increases in the numbers of colony-forming units in the BM and spleen of *Adam10/Mx1* mice compared with control mice (Figure 1J). Taken together, these observations show that conditional

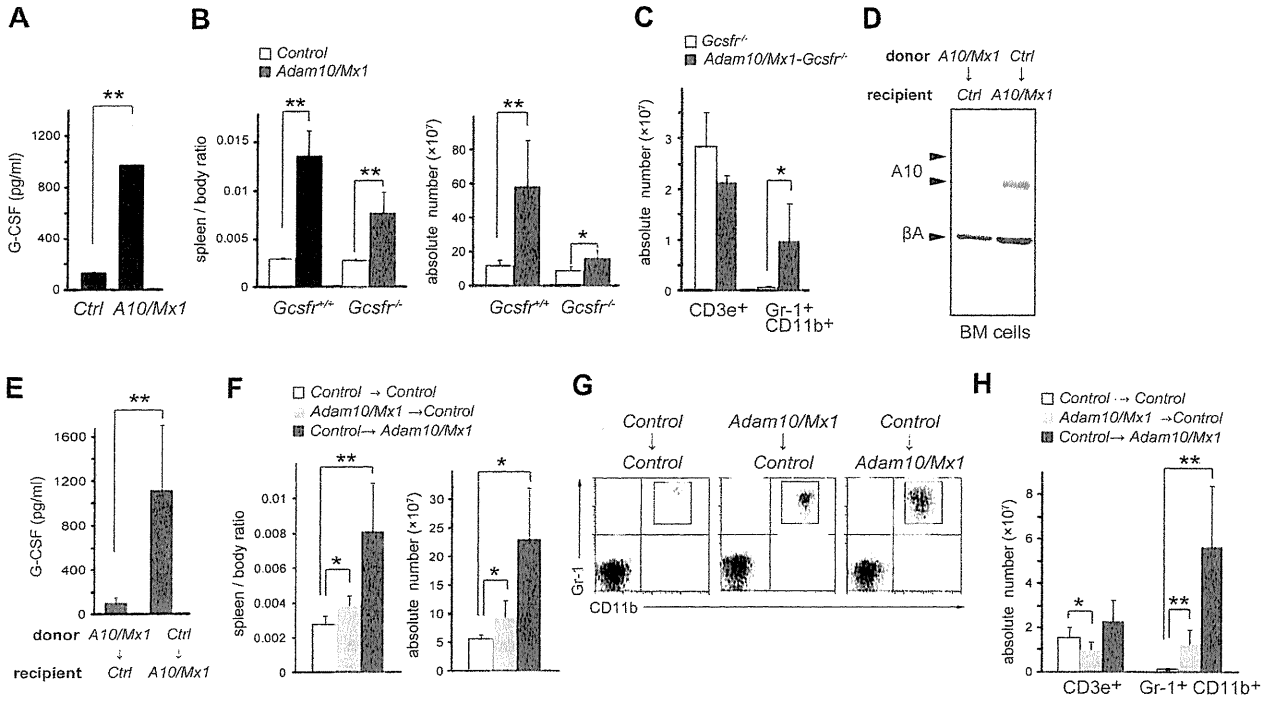

Figure 2. Dimorphic effects of ADAM10 on granulopoiesis. (A) Serum G-CSF levels in control (Ctrl) and *Adam10/Mx1* (*A10/Mx1*) mice evaluated by ELISA. Bars indicate mean ± SD (n = 5). (B) Spleen/body weight ratios and total cell counts in the spleen of control and *Adam10/Mx1* mice in either $Gcsf^{+/+}$ or $Gcsfr^{-/-}$ genetic background. Bars indicate mean ± SD (n = 4). (C) Numbers of $CD3e^+$ cells and $Gr\text{-}1^+$ $CD11b^+$ splenocytes in $Gcsfr^{-/-}$ and *Adam10/Mx1-Gcsfr*$^{-/-}$ mice. Bars indicate mean ± SD (n = 5). (D) Western blot analysis of ADAM10 (A10) and β-actin (βA) in BM cells from control (Ctrl) recipient mice reconstituted with *Adam10/Mx1* (*A10/Mx1*) BM cells and *Adam10/Mx1* recipient mice reconstituted with control BM cells. (E) Serum G-CSF levels in control (Ctrl) recipient mice reconstituted with *Adam10/Mx1* (*A10/Mx1*) BM cells and *Adam10/Mx1* recipient mice reconstituted with control BM cells. (F) Spleen/body weight ratios and total cell counts in the spleen of control recipient mice reconstituted with control BM cells, control recipient mice reconstituted with *Adam10/Mx1* BM cells, and *Adam10/Mx1* recipient mice reconstituted with control BM cells. Bars indicate mean ± SD (n = 10). Flow cytometric analysis (G) and total cell counts (H) of $Gr\text{-}1^+$ $CD11b^+$ cells and $CD3e^+$ cells in the spleen of control recipient mice reconstituted with control BM cells, control recipient mice reconstituted with *Adam10/Mx1* BM cells, and *Adam10/Mx1* recipient mice reconstituted with control BM cells. Note that there was also a decrease in a T-cell population ($CD3e^+$ cells) in the spleen of control recipient mice reconstituted with *Adam10/Mx1* cells (H), consistent with previous findings that the effect of Notch signaling in T-cell development is cell autonomous.[23] Bars indicate mean ± SD (n = 10). The flow cytometric analysis shown here is a representative result of 3 independent experiments. *t* test: $^*P < .05$, $^{**}P < .005$.

inactivation of ADAM10 leads to MPD. In addition, we found that T-cell development was impaired at an early stage of differentiation (supplemental Figure 2), similar to the case for conditional *Notch1*–knock-out mice.[23] In accordance with this, the transcript levels of the Notch target-genes (*Hes1*, *Hey1*, and *Hey2*) were significantly reduced in *Adam10/Mx1* mice (Figure 1K).

Both cell-autonomous and non–cell-autonomous ADAM10 activity affects granulopoiesis

We next performed a multiplex analysis of serum cytokines using antibody arrays and found that several cytokines, including G-CSF, were up-regulated in *Adam10/Mx1* mice (Figure 2A; supplemental Figure 3). Because G-CSF is a highly potent cytokine for stimulating granulopoiesis and progenitor cell proliferation, we hypothesized that aberrant production of G-CSF was the primary cause of MPD, as has been shown in different Notch signaling–defective mutant mice.[19] To test this hypothesis, we mated *Adam10/Mx1* mice with $Gcsfr^{-/-}$ mice[24] to block G-CSF receptor signaling. Unexpectedly, although the degree of splenomegaly and increase in granulopoiesis were significantly lessened, *Adam10/Mx1-Gcsfr*$^{-/-}$ double-mutant mice still developed splenomegaly (Figure 2B-C), which indicates that MPD in *Adam10/Mx1* mice was caused by G-CSF–dependent and G-CSF–independent mechanisms. We next performed reciprocal BM transfer experiments to determine the source of G-CSF. A nearly complete lack of ADAM10 expression in the BM cells in control recipient mice and positive ADAM10 expression in the BM cells in *Adam10/Mx1* recipient mice were confirmed at the time of euthanasia (Figure 2D). The serum level of G-CSF was up-regulated in *Adam10/Mx1* recipient mice reconstituted with control BM cells, whereas that in control mice reconstituted with *Adam10/Mx1* BM cells remained unaffected (Figure 2E). These findings indicate that a lack of ADAM10 in the host environment, but not in hematopoietic cells, leads to aberrant production of G-CSF. Furthermore, we found that not only *Adam10/Mx1* recipient mice reconstituted with control BM cells but also control recipient mice reconstituted with *Adam10/Mx1* cells developed splenomegaly and MPD (Figure 2F-H). These observations suggest that a lack of ADAM10 activity in the host environment leads to aberrant G-CSF production and ultimately results in MPD, whereas MPD caused by ADAM10-defective hematopoietic cells is not dependent on G-CSF. Therefore, ADAM10 has both cell-autonomous and non–cell-autonomous functions in granulopoiesis.

It has been shown that several Notch signaling–defective mice[17-20,25] develop a similar MPD phenotype as observed in the present study (supplemental Table 1). Although the targeted genes in these mutant lines are different in their participation in the Notch

signaling cascade and also have functions outside Notch signaling, they share a common feature in the MPD phenotype: that it is primarily derived from a non–cell-autonomous mechanism and is potentially dependent on aberrant production of G-CSF.[19] In this respect, a recent study showing that hematopoietic-specific inactivation of nicastrin, a component of the γ-secretase complex, results in a cell-autonomous, but not in non–cell-autonomous, MPD appears contradictory.[25] This discrepancy could be attributed to various factors, including the differences in the functions of the targeted genes and the temporal and spatial differences in gene disruption among these mutant lines. Analysis and comparison of the serum cytokine profiles (especially those involved in hematopoiesis, including G-CSF) among these mutant mice should provide a clue as to whether these Notch signaling–defective mice share a common mechanism behind the MPD phenotype.

In conclusion, the present study further supports ADAM10 as the relevant sheddase for Notch in vivo and reveals dimorphic effects of ADAM10 on granulopoiesis, in which ADAM10 in nonhematopoietic cells acts on granulopoiesis through regulation of G-CSF production, whereas ADAM10 in hematopoietic cells acts in a cell-autonomous and G-CSF–independent manner. In addition, because disruption of *Adam10* can potentially block all Notch signaling, the *Adam10*$^{flox/flox}$ mice described herein may serve as a useful tool for studying the functions of Notch signaling in vivo.

Acknowledgments

The authors thank Shizue Tomita, Kaori Sue, and Yuko Hashimoto for their technical assistance.

This work was supported in part by the Takeda Science Foundation, the Nakatomi Foundation, Keio University Kanrinmaru project, MEXT KAKENHI (21390424 and 23592230), and a grant from the Japanese Ministry of Health, Labor, and Welfare (H20-Nanchi-Ippan-032).

Authorship

Contribution: M.Y. performed research and analyzed data; T. Kimura and Y.O. performed histologic analysis; T.T., S.U., T. Koba, J.T., and H.M. performed parts of the research; M.M., K.C., and Y.T. supervised the project; D.C.L. provided *Gcsfr*$^{-/-}$ mice; and K.H. designed research, performed research, analyzed data, and wrote the manuscript.

Conflict-of-interest disclosure: The authors declare no competing financial interests.

Correspondence: Keisuke Horiuchi, The Department of Orthopedic Surgery, School of Medicine, Keio University, 35 Shinanomachi, Shinjuku-ku, Tokyo 160-8582, Japan; e-mail: horiuchi@z3.keio.jp.

References

1. Lai EC. Notch signaling: control of cell communication and cell fate. *Development.* 2004;131(5):965-973.
2. Weber JM, Calvi LM. Notch signaling and the bone marrow hematopoietic stem cell niche. *Bone.* 2010;46(2):281-285.
3. Yuan JS, Kousis PC, Suliman S, Visan I, Guidos CJ. Functions of Notch signaling in the immune system: consensus and controversies. *Annu Rev Immunol.* 2010;28:343-365.
4. Varnum-Finney B, Purton LE, Yu M, et al. The Notch ligand, Jagged-1, influences the development of primitive hematopoietic precursor cells. *Blood.* 1998;91(11):4084-4091.
5. Stier S, Cheng T, Dombkowski D, Carlesso N, Scadden DT. Notch1 activation increases hematopoietic stem cell self-renewal in vivo and favors lymphoid over myeloid lineage outcome. *Blood.* 2002;99(7):2369-2378.
6. Calvi LM, Adams GB, Weibrecht KW, et al. Osteoblastic cells regulate the haematopoietic stem cell niche. *Nature.* 2003;425(6960):841-846.
7. Varnum-Finney B, Xu L, Brashem-Stein C, et al. Pluripotent, cytokine-dependent, hematopoietic stem cells are immortalized by constitutive Notch1 signaling. *Nat Med.* 2000;6(11):1278-1281.
8. Mancini SJ, Mantei N, Dumortier A, Suter U, MacDonald HR, Radtke F. Jagged1-dependent Notch signaling is dispensable for hematopoietic stem cell self-renewal and differentiation. *Blood.* 2005;105(6):2340-2342.
9. Maillard I, Koch U, Dumortier A, et al. Canonical Notch signaling is dispensable for the maintenance of adult hematopoietic stem cells. *Cell Stem Cell.* 2008;2(4):356-366.
10. Brou C, Logeat F, Gupta N, et al. A novel proteolytic cleavage involved in Notch signaling: the role of the disintegrin-metalloprotease TACE. *Mol Cell.* 2000;5(2):207-216.
11. Peschon JJ, Slack JL, Reddy P, et al. An essential role for ectodomain shedding in mammalian development. *Science.* 1998;282(5392):1281-1284.
12. Horiuchi K, Kimura T, Miyamoto T, et al. TNFalpha-converting enzyme (TACE/ADAM17) inactivation in mouse myeloid cells prevents lethality from endotoxin shock. *J Immunol.* 2007;179(5):2686-2689.
13. Hartmann D, de Strooper B, Serneels L, et al. The disintegrin/metalloprotease ADAM 10 is essential for Notch signalling but not for alpha-secretase activity in fibroblasts. *Hum Mol Genet.* 2002;11(21):2615-2624.
14. Weber S, Niessen MT, Prox J, et al. The disintegrin/metalloproteinase Adam10 is essential for epidermal integrity and Notch-mediated signaling. *Development.* 2011;138(3):495-505.
15. Gibb DR, El Shikh M, Kang DJ, et al. ADAM10 is essential for Notch2-dependent marginal zone B cell development and CD23 cleavage in vivo. *J Exp Med.* 2010;207(3):623-635.
16. van Tetering G, van Diest P, Verlaan I, van der Wall E, Kopan R, Vooijs M. Metalloprotease ADAM10 is required for Notch1 site 2 cleavage. *J Biol Chem.* 2009;284(45):31018-31027.
17. Kim YW, Koo BK, Jeong HW, et al. Defective Notch activation in microenvironment leads to myeloproliferative disease. *Blood.* 2008;112(12):4628-4638.
18. Qyang Y, Chambers SM, Wang P, et al. Myeloproliferative disease in mice with reduced presenilin gene dosage: effect of gamma-secretase blockage. *Biochemistry.* 2004;43(18):5352-5359.
19. Dumortier A, Durham AD, Di Piazza M, et al. Atopic dermatitis-like disease and associated lethal myeloproliferative disorder arise from loss of Notch signaling in the murine skin. *PLoS One.* 2010;5(2):e9258.
20. Zhou L, Li LW, Yan Q, et al. Notch-dependent control of myelopoiesis is regulated by fucosylation. *Blood.* 2008;112(2):308-319.
21. Kühn R, Schwenk F, Aguet M, Rajewsky K. Inducible gene targeting in mice. *Science.* 1995;269(5229):1427-1429.
22. Osawa M, Hanada K, Hamada H, Nakauchi H. Long-term lymphohematopoietic reconstitution by a single CD34-low/negative hematopoietic stem cell. *Science.* 1996;273(5272):242-245.
23. Radtke F, Wilson A, Stark G, et al. Deficient T cell fate specification in mice with an induced inactivation of Notch1. *Immunity.* 1999;10(5):547-558.
24. Liu F, Wu HY, Wesselschmidt R, Kornaga T, Link DC. Impaired production and increased apoptosis of neutrophils in granulocyte colony-stimulating factor receptor-deficient mice. *Immunity.* 1996;5(5):491-501.
25. Klinakis A, Lobry C, Abdel-Wahab O, et al. A novel tumor-suppressor function for the Notch pathway in myeloid leukaemia. *Nature.* 2011;473(7346):230-233.

Published October 17, 2011

Correction

The Journal of Experimental Medicine

Osteoclasts are dispensable for hematopoietic stem cell maintenance and mobilization

Kana Miyamoto, Shigeyuki Yoshida, Miyuri Kawasumi, Kazuaki Hashimoto, Tokuhiro Kimura, Yuiko Sato, Tami Kobayashi, Yoshiteru Miyauchi, Hiroko Hoshi, Ryotaro Iwasaki, Hiroya Miyamoto, Wu Hao, Hideo Morioka, Kazuhiro Chiba, Takashi Kobayashi, Hisataka Yasuda, Josef M. Penninger, Yoshiaki Toyama, Toshio Suda, and Takeshi Miyamoto

Vol. 208, No. 11, October 24, 2011. Pages 2175–2181.

The authors regret that the dosage of RANKL and control antibodies used in the HSC mobilization experiments shown in Figure 6 were incorrectly reported in micrograms. The correct dosages were 5 mg/kg anti-RANKL and 2.5 mg/kg control antibody. The html and pdf versions of the article have been corrected.

J Orthop Sci (2011) 16:321–325
DOI 10.1007/s00776-011-0060-4

CASE REPORT

Arthroscopic removal of intra-articular osteoid osteoma in the knee: case report and review of the literature

Mitsuru Furukawa · Ukei Anazawa · Keisuke Horiuchi · Hiroo Yabe · Hideo Morioka · Makio Mukai · Takashi Toyoda · Kazuhiro Chiba · Tateru Shiraishi · Yoshiaki Toyama

Received: 17 November 2009 / Accepted: 8 June 2010 / Published online: 24 March 2011

Introduction

Osteoid osteoma is a relatively common benign bone tumor first described by Jaffe [1]. It most frequently arises in the long bones and exhibits a characteristic X-ray appearance, that is, a small radiolucent zone surrounded by reactive circumferential sclerosis (nidus) [2, 3]. Nocturnal pain, which can be alleviated by aspirin, is one of the characteristic clinical manifestations of this bone tumor [4]. Although it is relatively rare, osteoid osteoma can also arise in the intra-articular regions, and we found 14 such cases arising in the knee joint in the literature [5–18]. Patients with intra-articular osteoid osteoma often present with joint pain, intracapsular effusion, restricted motion, and muscle atrophy in the affected limb, which can be mistaken for more common entities, such as traumatic or degenerative pathologies of the joint. Furthermore, X-ray examination often fails to show the characteristic nidus that is typically seen in extra-articular osteoid osteoma and therefore can result in a delayed diagnosis. We herein present a case of intra-articular osteoid osteoma arising in the knee joint, which was successfully treated by arthroscopy, and review the reported cases of intra-articular osteoid osteoma arising in the knee.

M. Furukawa · U. Anazawa · K. Horiuchi · H. Yabe · H. Morioka · K. Chiba · Y. Toyama
Department of Orthopedic Surgery, School of Medicine, Keio University, Tokyo, Japan

U. Anazawa (✉) · T. Shiraishi
Department of Orthopedic Surgery, Tokyo Dental College Ichikawa General Hospital, Ichikawa, Japan
e-mail: ukei@tc4.so-net.ne.jp

M. Mukai
Department of Diagnostic Pathology, School of Medicine, Keio University, Tokyo, Japan

T. Toyoda
Nishi Waseda Orthopedic Surgery, Tokyo, Japan

Case report

A 23-year-old woman with a 2-year history of left knee pain visited our hospital. The pain was persistent even at rest and worsened at night. The use of non-steroidal anti-inflammatory drugs partially alleviated the pain. The patient had visited several clinics and had been treated conservatively; however, the treatments failed to improve her symptoms. Her medical and family histories were unremarkable. On physical examination, effusion and tenderness in the lateral side of the left knee were noted. The left thigh muscle was highly atrophic, whereas the range of motion remained intact. Laboratory findings revealed no abnormality. Radiographs of the left knee showed a radiolucent nidus-like lesion in the anterior distal femur with ill-defined marginal sclerosis (Fig. 1a, b). On magnetic resonance imaging (MRI), bone edema and a lesion resembling synovitis were found (Fig. 1c, d). Computed tomography (CT) of the left distal femur revealed a small cystic lesion approximately 8 mm in diameter in the anterior aspect of the lateral femoral condyle (Fig. 1e, f), which was not apparent on the MRI. In addition, bone scintigraphy revealed marked uptake in the distal femur but not in other skeletal bones (Fig. 1g). Based on these findings, we made a diagnosis of intra-articular osteoid osteoma arising in the distal femur and planned an arthroscopic excision of the lesion.

Since the lesion was located in the anterolateral cortex of the distal femoral metaphysis, a superolateral portal was

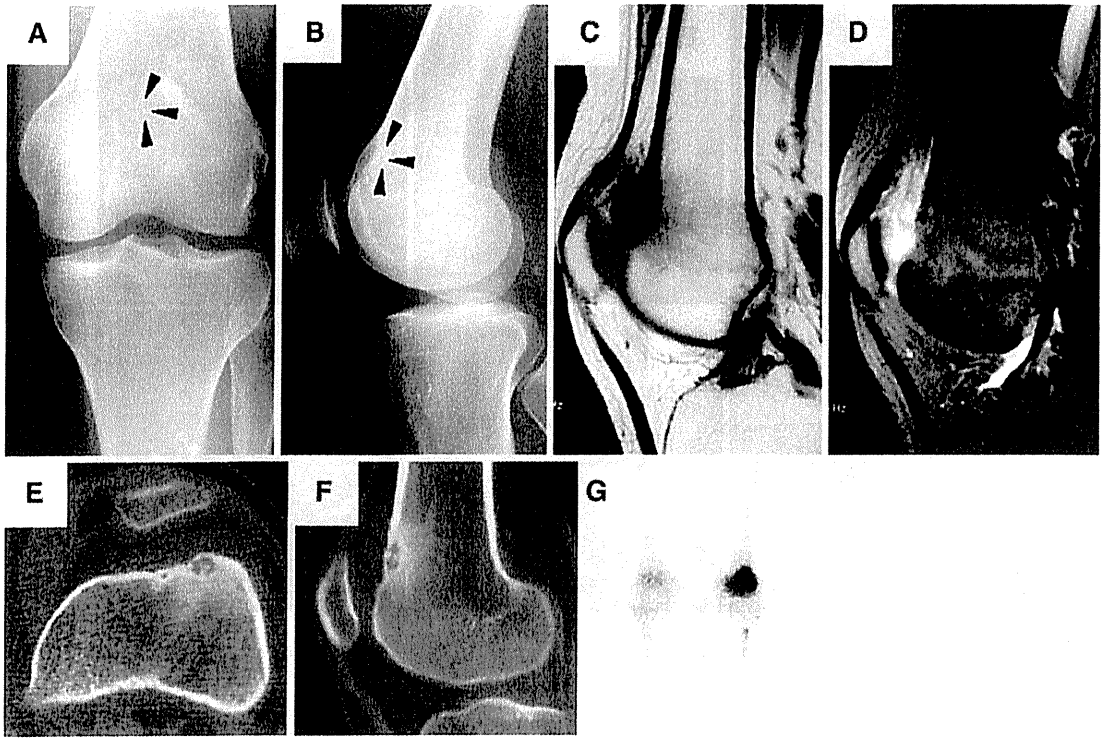

Fig. 1 X-rays of the distal femur (**a**, **b** *arrowheads*). T1 (**c**) and T2 (**d**) weighted MRI images. **e**, **f** CT images revealed the nidus in the lateral condyle. **g** Technetium bone scintigraphy

used for arthroscopic instrumentation in addition to the standard anteromedial and anterolateral portals. Under arthroscopy, edematous hypervascularized synovium was observed in the anterolateral aspect of the femur, adjacent to the proximal border of the articular cartilage of patellar groove (Fig. 2a). No abnormalities were seen in the meniscuses or ligaments. After removal of the swollen synovium, a lesion with osseous prominence was identified, which indicated the location of the nidus (Fig. 2b). The underlying cortex was found to be edematous and rough on the surface (Fig. 2c). A bone plug was harvested using a surgical chisel from the lesion, approximately 2 cm proximal to the border of the cartilage of the patellar groove and 1 cm medial to the lateral edge of the femur (Fig. 2d). The location was determined by reference to the preoperative CT images (Fig. 1e, f). The bone tissue that remained after the bone plug was removed contained edematous bone and whitish calcified tissue, indicating that the nidus had not been fully removed with the chisel. Therefore, the lesion was further curetted carefully using a chisel and a motorized burr (Fig. 2e, f). A complete removal of the lesion was also confirmed by perioperative radiography.

Pathological examination of the surgical specimen confirmed the diagnosis of osteoid osteoma. The nidus surrounded by sclerotic reactive bone was observed, and high magnification showed that the nidus was composed of osteoid and woven bone lined by osteoblasts, and filled with fibrous cells and vessels (Fig. 3a). The postoperative course was uneventful, and the pain was relieved immediately after the surgery (Fig. 3b). The defect appeared less conspicuous on the X-ray 2 years after surgery (Fig. 3c). At the 2-year follow-up point, the patient is asymptomatic without any sign of recurrence.

Discussion

Osteoid osteoma is a benign osteoblastic tumor with a distinctive histology characterized by vascular osteoid tissue surrounded by sclerotic bone (nidus) [19]. Although osteoid osteoma is typically found in the metaphysis and shaft of long bones, it can arise in any part of the skeleton, including in periarticular and intra-articular regions. Osteoid osteoma of the knee joint is relatively uncommon, and our search of the literature turned up only 14 reported cases. The diagnosis of intra-articular osteoid osteoma is often difficult, and the time between the onset of the symptoms and the final diagnosis can be quite long (see Table 1). The reasons for the delayed diagnosis, in addition to the rarity of this disorder in the joint, include its nonspecific clinical presentation, which resembles other more

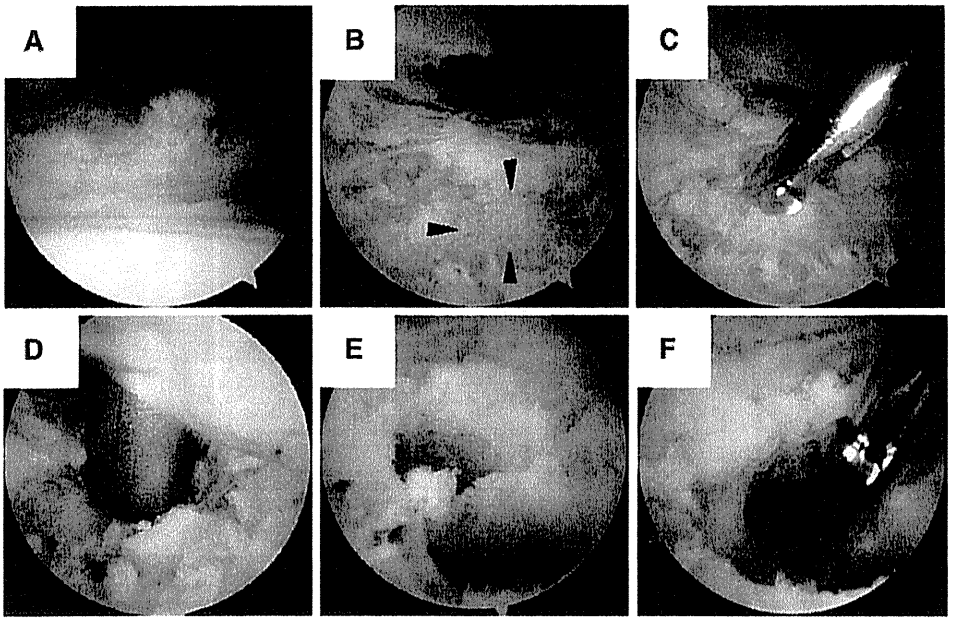

Fig. 2 Arthroscopic appearance of lesion. **a** Localized synovitis. **b** A lesion with osseous prominence (*arrowheads*). **c** Bulging cortical bone marked by abrader burr. **d** Bone plug harvested by surgical chisel. Additional resection with chisel (**e**) and abrader burr (**f**)

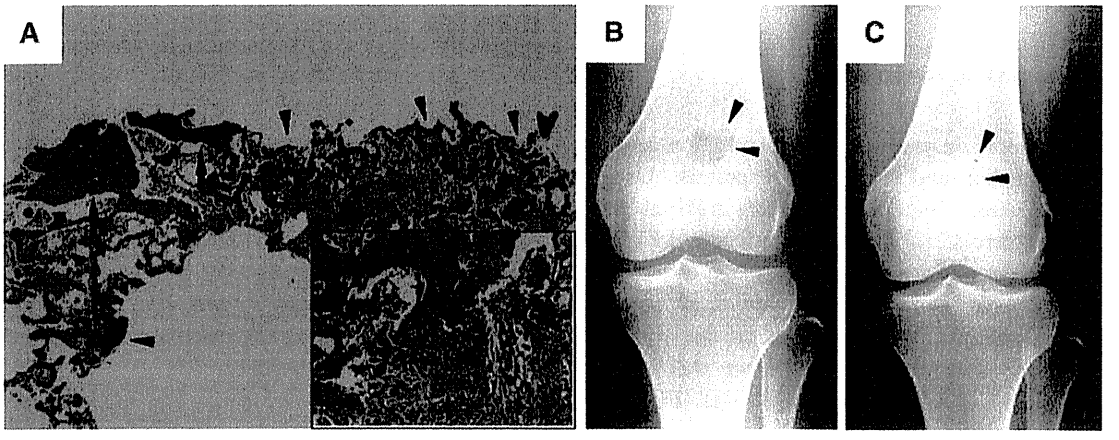

Fig. 3 Microscopy of specimen. **a** Nidus (*arrowheads*) surrounded by sclerotic reactive bone (*arrows*). *Insert* shows high-magnification view. **b** Postoperative X-ray showing radiolucent defect in the distal femur (*arrowheads*). **c** The defect 2 years after surgery (*arrowheads*)

common conditions, such as osteoarthritis and knee injuries, and the comparatively less conspicuous sclerotic bone lesion on X-rays compared with osteoid osteoma arising in the bone shaft. On the other hand, characteristic nocturnal pain alleviated by aspirin, a common and distinguishing symptom in patients with regular (extra-articular) osteoid osteoma, is seen in all the reported cases of osteoid osteoma arising in the knee joint, without exception [5–18].

Therefore, when a clinician encounters a young patient with persistent nocturnal knee pain and without a history of trauma, further clinical imaging may be advised, even if a typical nidus or sclerotic lesion is not seen on X-rays. MRI may be helpful in some cases, but bone and soft-tissue edema, in addition to joint effusion in cases of intra-articular osteoid osteoma, are frequent and may disguise the nidus. Bone scintigraphy is highly sensitive for identifying osteoid osteoma; however, it is, in general, a non-specific modality that gives a positive signal for any lesion with abnormal bone formation and/or bone perfusion. Therefore, it is mandatory to identify the nidus by CT examinations, especially in cases of intra-articular osteoid osteoma, in which the sclerotic lesion surrounding the nidus is often inconspicuous by routine X-rays, to make the correct diagnosis.

The treatments for osteoid osteoma in the knee joint include open surgery [5, 7, 8], open surgery with

Table 1 Summary of the reported cases of osteoid osteoma arising in the knee joint ([4–17] and the current report; total = 15 cases)

Characteristics	
Age of onset (average)	22.5 years old
Sex	
Male	10 cases
Female	4 cases
Not described	1 case
Duration for diagnosis (average)	22.5 months
Symptoms	
Nocturnal pain	15 cases
Limited ROM	5 cases
Joint effusion	2 cases
Atrophy of quadriceps muscle	6 cases
X-rays and laboratory examinations	
Identification of nidus on X-rays	5 cases
Surgery	
Arthroscopic resection	4 cases
Open surgery (cryoablation, 1 case)	4 cases
CT-guided resection (RFA, 1 case)	3 cases
Not described	4 cases
Recurrence/complications	None

cryoablation [6], CT-guided radio-frequency ablation (RFA) [10], CT-guided curette [9, 11], and arthroscopic resection [12–14] (Table 1). Pain relief was immediate upon removal of the lesion in all cases in the literature, and there was no apparent difference in the clinical outcome irrespective of the selected surgical treatment. Of note, patients with a lesion arising in the femur were treated either with arthroscopic excision or open surgery, but not with CT-guided curette, while those with a lesion arising in the tibia were all treated by CT-guided curette. Compared with open surgery with or without cryoablation, it is evident that arthroscopic resection is less invasive and should be considered when treating patients with osteoid osteoma in the knee joint. However, a limitation in the availability of portal sites and accessibility to the lesion may preclude the wider application of arthroscopic excision.

CT-guided methods, either with RFA or curette, are also relatively non-invasive and have a favorable clinical outcome with a relatively low recurrence rate for osteoid osteomas (RFA 5.5–11%, curette 5.1–12.5%) [3, 20]. However, CT-guided methods can have limitations: they require assistance from a radiologist, and the procedure has to be performed in a CT room (or a surgery room equipped with a CT scan), which may not be available in all clinical settings. RFA may also cause the degeneration of cartilage when used to resect subchondral osteoid osteomas. Since arthroscopic methods are more feasible in terms of equipment availability, and since other lesions (such as meniscus injuries) that can cause joint pain can be examined and treated during the same procedure, arthroscopic methods are advantageous over CT-guided methods for cases of articular lesion.

Recurrent pain due to incomplete excision is a relatively common complication in patients with osteoid osteoma. Even with CT-guided methods, recurrent pain occurs in 5–24% of the cases [21, 22]. Other complications, including osteomyelitis, fracture, and skin burn, are also occasionally observed in patients treated with CT-guided methods (1.7–12.5% of cases) [21, 23–25]. Although to date there are far fewer reported cases in which arthroscopic excision was used compared with CT-guided methods, none of the patients treated with arthroscopic excision required further treatment or experienced serious complications. Therefore, arthroscopic excision is at least as effective as CT-guided methods for identifying and removing the lesion. The reason for this favorable outcome is not yet clear, but it may be because arthroscopic methods usually allow the surgeon to visualize the lesion in detail, thereby making the complete removal of the symptomatic nidus easier, without causing damage to the surrounding tissue, compared with other, conventional methods.

The diagnosis of osteoid osteoma, as we have discussed, is often difficult, especially in cases in which typical features are obscured on clinical images. Sans et al. [24] reported that, of 38 cases that were initially diagnosed as osteoid osteoma on clinical images and treated by CT-guided curettage, pathological examination resulted in a different diagnosis for six of them, including mucoid cysts, fibrous dysplasia, fibromucoid lesion, focal osteochondritis, and osteomyelitis. A definite diagnosis of osteoid osteoma, therefore, cannot be made solely on the basis of clinical images, and pathological examination is also required. However, it is often difficult to obtain a large enough specimen for pathological diagnosis by using CT-guided methods.

According to the reported summaries of osteoid osteoma cases treated with CT-guided methods, a definite pathological diagnosis was achieved in only 36–79% of them, depending on the cases included [21, 26]. On the other hand, as shown in our case, surgical specimens can be straightforwardly obtained in arthroscopy-assisted methods, since the location of the lesion can be directly confirmed arthroscopically during the procedure. This is another advantage of arthroscopy-assisted over CT-assisted methods or other methods that involve the in situ destruction of the lesion (either by RFA or open surgery with cryoablation). Nevertheless, given the paucity of clinical data on arthroscopic excision, further studies will be necessary to determine whether (and under what conditions) this method should be the clinical modality of

choice for treating intra-articular osteoid osteoma in the knee joint.

In summary, here we presented a case of osteoid osteoma arising in the knee joint that was successfully treated with arthroscopic excision. Although the diagnosis of intra-articular osteoid osteoma is often challenging, with a careful history questionnaire and the knowledge that articular osteoid osteoma frequently lacks the characteristic sclerotic lesion and nidus on plain X-rays, a correct diagnosis can be achieved. The clinical value of arthroscopic excision for osteoid osteoma arising in the knee joint is not yet conclusive; however, our case and others suggest that this option should be considered, especially for lesions arising in the femoral condyle, where arthroscopy can be performed without difficulty.

References

1. Jaffe HL. Osteoid osteoma of bone. Radiology. 1935;45:319.
2. Klein MH, Shankman S. Osteoid osteoma: radiologic and pathologic correlation. Skeletal Radiol. 1992;21:23–31.
3. Sierre S, Innocenti S, Lipsich J, Lanfranchi L, Questa H, Moguillansky S. Percutaneous treatment of osteoid osteoma by CT-guided drilling resection in pediatric patients. Pediatr Radiol. 2006;36:115–8.
4. Kattapuram SV, Kushner DC, Phillips WC, Rosenthal DI. Osteoid osteoma: an unusual cause of articular pain. Radiology. 1983;147:383–7.
5. Odaka T, Koshino T, Saito T. Intraarticular epiphyseal osteoid osteoma of the distal femur. J Pediatr Orthop. 1987;7:331–3.
6. Vallianatos PG, Tilentzoglou AC, Seitaridis SV, Mahera HJ. Osteoid osteoma of the patella: a case report. Knee Surg Sports Traumatol Arthrosc. 2006;14:161–4.
7. Hanada H, Ogata K, Hara M, Emoto G, Fujiwara A. Clinical study of osteoid osteoma of the lateral femoral condyle. Kansetsukyou. 1999;24:175–9 (in Japanese).
8. Torg JS, Loughran T, Pavlov H, Schwamm H, Gregg J, Sherman M, Balduini FC. Osteoid osteoma. Distant, periarticular, and subarticular lesions as a cause of knee pain. Sports Med. 1985;2:296–304.
9. Franceschi F, Marinozzi A, Papalia R, Longo UG, Gualdi G, Denaro E. Intra- and juxta-articular osteoid osteoma: a diagnostic challenge: misdiagnosis and successful treatment: a report of four cases. Arch Orthop Trauma Surg. 2006;126:660–7.
10. Eggel Y, Theumann N, Luthi F. Intra-articular osteoid osteoma of the knee: clinical and therapeutical particularities. Joint Bone Spine. 2007;74:379–81.
11. Franceschi F, Longo UG, Ruzzini L, Marinozzi A, Rizzello G, Papalia R, Denaro V. En-bloc retrograde resection of an osteoid osteoma of the patella using computed tomography under arthroscopic control. J Knee Surg. 2008;21:136–40.
12. Abnousi F, Saliman JD, Fanton GS. Arthroscopic visualization and assisted excision of osteoid osteoma at the knee: a case report and review. Am J Sports Med. 2008;36:375–8.
13. Gunes T, Erdem M, Bostan B, Sen C, Sahin SA. Arthroscopic excision of the osteoid osteoma at the distal femur. Knee Surg Sports Traumatol Arthrosc. 2008;16:90–3.
14. Yamashita M, Sasho T, Wada Y, Nakagawa K, Fujita K, Takahashi K, et al. A case of osteoid osteoma excised arthroscopically at the knee joint. Kansetsukyou. 2000;25:183–7 (in Japanese).
15. Georgoulis AD, Soucacos PN, Beris AE, Xenakis TA. Osteoid osteoma in the differential diagnosis of persistent joint pain. Knee Surg Sports Traumatol Arthrosc. 1995;3:125–8.
16. Heuijerjans W, Dandy DJ, Harris D. Arthroscopic excision of an intra-articular osteoid osteoma at the knee. Arthroscopy. 1986;2:215–6.
17. Szendroi M, Kollo K, Antal I, Lakatos J, Szoke G. Intraarticular osteoid osteoma: clinical features, imaging results, and comparison with extraarticular localization. J Rheumatol. 2004;31:957–64.
18. Merzoung V, Adamsbaum C. Cas radiologique: radiological case study. Arch Pediatr. 2005;12:1551–3.
19. Carrie YI, Andrew LF, John RG. Bone-forming tumors, chap. 14. In: Bone and soft tissue pathology. Amsterdam: Elsevier; 2009. p. 313–6.
20. Fenichel I, Garniack A, Morag B, Palti R, Salai M. Percutaneous CT-guided curettage of osteoid osteoma with histological confirmation: a retrospective study and review of the literature. Int Orthop. 2006;30:139–42.
21. Vanderschueren GM, Taminiau AH, Obermann WR, Bloem JL. Osteoid osteoma: clinical results with thermocoagulation. Radiology. 2002;224:82–6.
22. Rosenthal DI, Hornicek FJ, Torriani M, Gebhardt MC, Mankin HJ. Osteoid osteoma: percutaneous treatment with radiofrequency energy. Radiology. 2003;229:171–5.
23. Cioni R, Armillotta N, Bargellini I, Zampa V, Cappelli C, Vagli P, Boni G, Marchetti S, Consoli V, Bartolozzi C. CT-guided radiofrequency ablation of osteoid osteoma: long-term results. Eur Radiol. 2004;14:1203–8.
24. Sans N, Galy-Fourcade D, Assoun J, Jarlaud T, Chiavassa H, Bonnevialle P, Railhac N, Giron J, Morera-Maupomé H, Railhac JJ. Osteoid osteoma: CT-guided percutaneous resection and follow-up in 38 patients. Radiology. 1999;212:687–92.
25. Gebauer B, Tunn PU, Gaffke G, Melcher I, Felix R, Stroszczynski C. Osteoid osteoma: experience with laser- and radiofrequency-induced ablation. Cardiovasc Interv Radiol. 2006;29:210–5.
26. Assoun J, Railhac JJ, Bonnevialle P, Poey C, Salles de Gauzy J, Baunin C, Cahuzac JP, Clement JL, Coustets B, Railhac N. Osteoid osteoma: percutaneous resection with CT guidance. Radiology. 1993;188:541–7.

JOURNAL OF MEDICAL CASE REPORTS

CASE REPORT Open Access

Natural evolution of desmoplastic fibroblastoma on magnetic resonance imaging: a case report

Yusaku Kamata[1], Ukei Anazawa[1*], Hideo Morioka[1], Takeshi Morii[2], Keiko Miura[1], Makio Mukai[3], Hiroo Yabe[1] and Yoshiaki Toyama[1]

Abstract

Introduction: Desmoplastic fibroblastoma (collagenous fibroma) is a recently described tumor thought to arise predominantly from subcutaneous tissue or skeletal muscle. The natural evolution of this tumor on magnetic resonance imaging has never been described, to the best of our knowledge. We herein report a case of desmoplastic fibroblastoma arising in the thigh and show the longitudinal magnetic resonance imaging findings.

Case presentation: A 60-year-old Japanese man presented with swelling of the medial side of his right thigh, and he complained of nighttime pain and slight tenderness. Magnetic resonance imaging demonstrated a 4 × 4 cm mass in the right thigh. Open biopsy was performed. The mass was diagnosed histologically as a benign fibrous tumor, and we maintained follow-up without surgical therapy. After one year, magnetic resonance imaging showed an increase in tumor size to 4 × 5 cm, but the histologic findings were the same as those obtained one year earlier. Resection was performed with narrow surgical margins. Pathologic diagnosis was desmoplastic fibroblastoma. Two years after surgery, the patient is free from pain and shows no signs or symptoms of recurrence.

Conclusion: The natural evolution of desmoplastic fibroblastoma is characterized by no changes in patterns on magnetic resonance imaging despite increasing size. This finding is clinically helpful for distinguishing desmoplastic fibroblastoma with increasing pain from the desmoid tumor.

Introduction

In 1995, Evans [1] first described desmoplastic fibroblastoma, a unique fibrous soft tissue tumor comprising spindle-shaped to stellate fibroblastic cells sparsely distributed in a dense fibrous background. This tumor, alternatively called *collagenous fibroma* [2], was clinically and morphologically distinct, as well as completely benign in previously reported series. Details of magnetic resonance imaging (MRI) findings for this tumor have been described for three cases [3,4], but the natural evolution of this tumor has never been described. Here, we present the natural evolution of this tumor on MRI.

Case presentation

A 60-year-old Japanese man presented with swelling of the medial side of his right thigh and complained of night pain and slight tenderness. Palpation disclosed a hard, well-circumscribed, mobile tumor. Otherwise healthy, he had no history of trauma to the thigh. The results of routine laboratory studies were normal.

MRI demonstrated a 4 × 4 cm mass in the right thigh, occupying a space between the vastus medialis, sartorius and semimembranosus muscles (Figure 1A, B). Open biopsy was performed. Because the mass was diagnosed histologically as a benign fibrous tumor, we maintained follow-up without surgical therapy. After one year, MRI showed an increase in tumor size to 4 × 5 cm. T1-weighted images characterized the mass as well-circumscribed and inhomogeneous, with signals predominantly isointense with muscle, but including several areas of low signal intensity (SI) (Figure 2A). On T2-weighted images, the mass predominantly showed low SI with scattered high-SI areas (Figure 2B). These MRI findings were the same as those obtained one year previously except for tumor size. T1-weighted images after contrast agent administration revealed heterogeneous enhancement of the lesion. Nonenhanced areas corresponded to regions with low SI on noncontrast T1-weighted images

* Correspondence: ukei@tc2.so-net.ne.jp
[1]Department of Orthopaedic Surgery, Keio University, 35 Shinanomachi, Shinjuku-ku, Tokyo 160-8582, Japan
Full list of author information is available at the end of the article

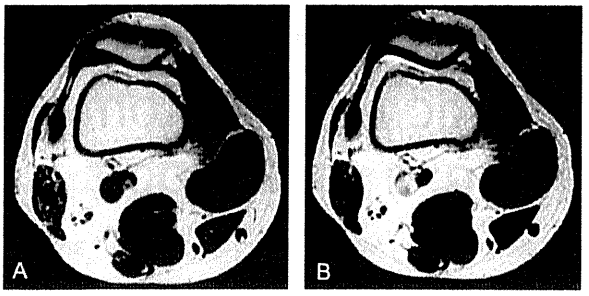

Figure 1 Magnetic resonance imaging findings, July 2001. A) Axial T1-weighted image (TR/TE: 500/14) showing a 4 × 4 cm, well-circumscribed, inhomogeneous mass as predominantly isointense with muscle containing areas of low signal intensity (SI). **B)** Axial T2-weighted image (TR/TE: 4000/105) showing scattered areas of high SI within low overall SI.

(Figure 2C). Based on this growth, with pain and enhancement of the lesion, resection was performed with narrow surgical margins; the tumor adjoined the vastus medialis, sartorius and semimembranosus muscles and was adjacent to Hunter's canal with fibrous adhesion to the adductor magnus tendon.

Pathologically, the tumor showed well-circumscribed borders and low vascularity (Figure 3A). Spindle-shaped and stellate fibroblastic cells were sparsely distributed in a dense fibrous background. In some myxocollagenous areas, cellularity was greater than in the fibrous area (Figure 3A, B). No mitotic figures were seen. The pathologic diagnosis was desmoplastic fibroblastoma.

At the most recent follow-up examination two years after surgery, the patient was free from pain and showed no signs or symptoms of recurrence.

Discussion

Evans [1] used the designation *desmoplastic fibroblastoma* when he described seven patients having masses with distinct morphologic characteristics. Subsequently, Nielsen *et al.* [2] reported seven other cases and proposed that the tumor be renamed *collagenous fibroma*, arguing that *desmoplastic fibroblastoma* misleads the reader into believing that the lesion consists of immature tumor cells inducing a desmoplastic response in host tissues.

These neoplasms typically occur in the fifth or sixth decades of life and occur two and a half times more often in men than women. Clinically, desmoplastic fibroblastoma presents as a firm, mobile, slowly growing mass located in subcutaneous tissue or near the deep aspect of skeletal muscles. Common locations include the arm, shoulder, posterior neck and upper back [1-8]. Few previous reports have described tumors arising in the thigh [1,2,6,8]. In the present patient, the tumor appeared to arise from the fascia of the thigh muscles. Such tumors located in the intermuscular space have not been described. The mass is usually painless; however, our patient complained of pain, as have those in some previous reports [3,5,6]. In our case, location of the tumor adjacent to Hunter's canal may have contributed to pain by compressing the saphenous nerve in the canal.

Previous authors recommended treatment of desmoplastic fibroblastoma by total surgical excision. No tumor recurrence during follow-up has been reported, including the present case.

On MRI, T1-weighted images of the mass depicted a mixture of low SI and isointensity. With T2-weighting, the mass showed scattered high-SI areas within a zone of low SI. Contrast T1-weighted images demonstrated inhomogeneous enhancement after contrast administration, and nonenhanced areas corresponding to regions showing low SI on noncontrast T1-weighted images. The size of the tumor increased over the course of one year, but the MRI findings of the tumor showed no changes.

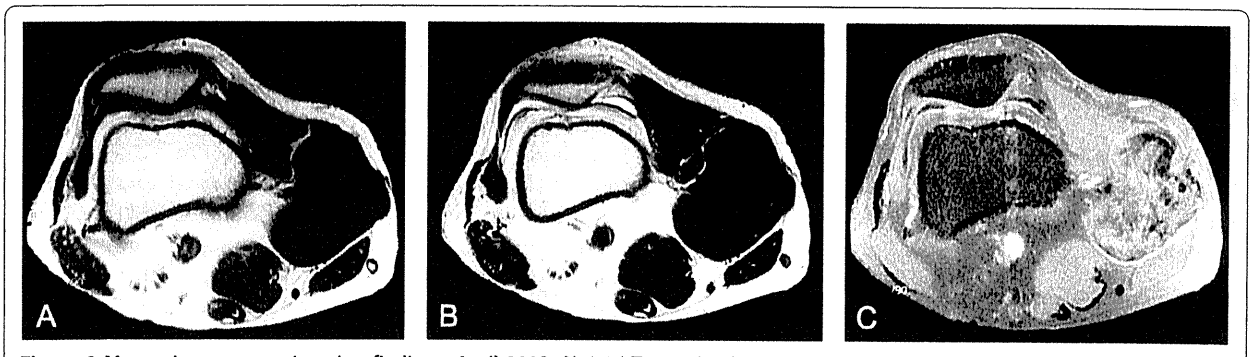

Figure 2 Magnetic resonance imaging findings, April 2002. A) Axial T1-weighted image (TR/TE: 500/8.6) showing an increasing size and the same pattern as one year previously. **B)** Axial T2-weighted image (TR/TE: 4000/104) showing the same ratio of high signal intensity (SI) area as in previous images. **C)** Axial postcontrast T1-weighted image (TR/TE: 500/8.6) showing nonenhanced areas that correspond to those showing low SI in precontrast T1-weighted images.

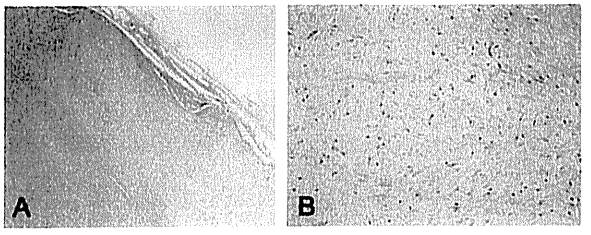

Figure 3 Pathologic findings (hematoxylin and eosin stain). A) Low-power photomicrograph of the tumor demonstrating fibrous and myxocollagenous areas. The tumor border is well defined. Fibrous area demonstrates wavy and dense collagen fibers. Cellularity is very low, consisting of spindle-shaped and stellate tumor cells. **B)** High-power photomicrograph of the area showing a myxocollagenous stroma, demonstrating benign-appearing spindle cells presenting higher cellularity than in the fibrous area.

Several reports have described the MRI appearance of this tumor, but in only three cases have MRI findings been described in detail [3,4], and those findings have varied. T1-weighted findings were described as having diverse SI, low SI compared with muscle, scattered isointense areas [4], and isointense areas with scattered areas of low and high SI [3]. T2-weighted findings also have varied among cases, including high-SI areas with small low-SI areas [4] and low-SI areas with small high-SI areas [3]. Postcontrast T1-weighted images have only been described in two cases. They showed enhanced areas within areas of low SI, and enhanced areas showed strong enhancement in one case, with inhomogeneous enhancement seen in the other case [3,4].

In previous reports, the relationship between MRI findings and histologic findings has been described. On T2-weighted images, low-SI areas correspond to abundant collagen fibers [3,4,9], and high-SI areas showing marked enhancement on contrast T1-images correspond to those histologically consisting of fibroblasts and loose collagen fibers [4]. On T1-weighted images, low-SI areas represent areas with low cellularity and abundant collagen fibers [3].

These reports indicate that MRI findings vary among and within individual tumors because of the variable cellularity.

Evans [1] suggested that the most significant differential diagnostic consideration was desmoid tumor because it may have similar cytologic features and is often locally aggressive.

On the other hand, Marco *et al.* [10] reported that desmoplastic fibroblastoma is a myofibroblastic lesion ultrastructurally demonstrating the presence of fibronexus junctions; markers of myofibroblastic differentiation, typically present on the cytoplasmic membrane of the cells, while desmoid tumor is fibroblastic. This ultrastructural finding is important in the differential diagnosis between desmoplastic fibroma and desmoid tumor.

Details of imaging studies of desmoid tumors have been well documented in previous reports [11-13], and the margins of the tumor are mostly ill defined. However, some MRI findings of desmoid tumor are similar to those of desmoplastic fibroblastoma [11,12]. Several reports have described desmoid tumors as resulting in pain [14], and Agrawal *et al.* [15] reported an increasing desmoid tumor with pain. When desmoplastic fibroblastoma increases with pain, such as in our case, the tumor needs to be distinguished from desmoid tumor.

The natural evolution of desmoid tumor has been documented [13], but that of desmoplastic fibroblastoma has not been previously reported. Vandevenne *et al.* [13] described the MRI findings of the natural evolution of desmoid tumors. Desmoid tumors showing high SI on T2-weighted images tend to increase in size. Subsequently, they show an increase in areas of low SI on T2-weighted images. Finally, they acquire an overall low SI both on T1- and T2-weighted images and decrease in size. In contrast, the MRI findings of desmoplastic fibroblastoma in our case showed an increase in tumor size, with the same pattern: mainly low SI on T1-weighted images. The follow-up period of one year and the two sets of MRIs may not be sufficient to understand the true behavior of slow-growing tumors, such as desmoplastic fibroblastoma. Clinically, however, changes in MRI findings provide important information in distinguishing between aggressive and slow-growing tumors.

Conclusion

This case study has described the MRI findings of desmoplastic fibroblastoma in relation to its natural evolution. The natural evolution of desmoplastic fibroblastoma is characterized by no change in patterns on MRI despite increasing size. This finding is clinically helpful for distinguishing desmoplastic fibroblastoma with increasing pain from desmoid tumor.

Consent

Written informed consent was obtained from the patient for publication of this case report and accompanying images. A copy of the written consent is available for review by the Editor-in-Chief of this journal.

Author details
[1]Department of Orthopaedic Surgery, Keio University, 35 Shinanomachi, Shinjuku-ku, Tokyo 160-8582, Japan. [2]Department of Orthopaedic Surgery, Kyorin University, 6-20-2 Shinkawa, Mitaka, Tokyo 181-8611, Japan. [3]Department of Diagnostic Pathology, Keio University Hospital, 35 Shinanomachi, Shinjuku-ku, Tokyo 160-8582, Japan.

Authors' contributions
YK drafted the manuscript and reviewed the literature. UA supervised treatment of the patient, carried out the patient's surgery and revised the manuscript. MM performed the histopathological analysis and helped draft the manuscript. HM, TM, KM, HY and TY helped draft the manuscript. All authors have read and approved the final manuscript.

Competing interests
The authors declare that they have no competing interests.

Received: 19 September 2009 Accepted: 7 April 2011
Published: 7 April 2011

References

1. Evans HL: **Desmoplastic fibroblastoma. A report of seven cases.** *Am J Surg Pathol* 1995, **19**:1077-1081.
2. Nielsen GP, O'Connell JX, Dickersin GR, Rosenberg AE: **Collagenous fibroma (desmoplastic fibroblastoma): a report of seven cases.** *Mod Pathol* 1996, **9**:781-785.
3. Ogose A, Hotta T, Emura I, Higuchi T, Kusano N, Saito H: **Collagenous fibroma of the arm: a report of two cases.** *Skeletal Radiol* 2000, **29**:417-420.
4. Shuto R, Kiyosue H, Hori Y, Miyake H, Kawano K, Mori H: **CT and MR imaging of desmoplastic fibroblastoma.** *Eur Radiol* 2002, **12**:2474-2476.
5. Beggs I, Salter DS, Dorfman HD: **Synovial desmoplastic fibroblastoma of hip joint with bone erosion.** *Skeletal Radiol* 1999, **28**:402-406.
6. Hasegawa T, Shimoda T, Hirohashi S, Hizawa K, Sano T: **Collagenous fibroma (desmoplastic fibroblastoma): report of four cases and review of the literature.** *Arch Pathol Lab Med* 1998, **122**:455-460.
7. Miettinen M, Fetsch JF: **Collagenous fibroma (desmoplastic fibroblastoma): a clinicopathologic analysis of 63 cases of a distinctive soft tissue lesion with stellate-shaped fibroblasts.** *Hum Pathol* 1998, **29**:676-682.
8. Sciot R, Samson I, van den Berghe H, Van Damme B, Dal Cin P: **Collagenous fibroma (desmoplastic fibroblastoma): genetic link with fibroma of tendon sheath?** *Mod Pathol* 1999, **12**:565-568.
9. Dinauer PA, Brixey CJ, Moncur JT, Fanburg-Smith JC, Murphey MD: **Pathologic and MR imaging features of benign fibrous soft-tissue tumors in adults.** *Radiographics* 2007, **27**:173-187.
10. Alberghini M, Pasquinelli G, Zanella L, Bacchini P, Bertoni F: **Desmoplastic fibroblastoma: a light and ultrastructural description of two cases.** *Ultrastruct Pathol* 2004, **28**:149-157.
11. Hartman TE, Berquist TH, Fetsch JF: **MR imaging of extraabdominal desmoids: differentiation from other neoplasms.** *AJR Am J Roentgenol* 1992, **158**:581-585.
12. Papagelopoulos PJ, Mavrogenis AF, Mitsiokapa EA, Papaparaskeva KT, Galanis EC, Soucacos PN: **Current trends in the management of extra-abdominal desmoid tumours.** *World J Surg Oncol* 2006, **3**:4-21.
13. Vandevenne JE, De Schepper AM, De Beuckeleer L, Van Marck E, Aparisi F, Bloem JL, Erkorkmaz Z, Brijs S: **New concepts in understanding evolution of desmoid tumors: MR imaging of 30 lesions.** *Eur Radiol* 1997, **7**:1013-1019.
14. Rock MG, Pritchard DJ, Reiman HM, Soule EH, Brewster RC: **Extra-abdominal desmoid tumors.** *J Bone Joint Surg Am* 1984, **66**:1369-1374.
15. Agrawal PS, Jagtap SM, Mitra SR: **Extra-abdominal desmoid tumour of the leg.** *Singapore Med J* 2008, **49**:e6-e7.

doi:10.1186/1752-1947-5-139
Cite this article as: Kamata *et al.*: Natural evolution of desmoplastic fibroblastoma on magnetic resonance imaging: a case report. *Journal of Medical Case Reports* 2011 **5**:139.

Case Reports in Oncology

Case Rep Oncol 2011;4:125–131
DOI: 10.1159/000325399

Published online:
March 4, 2011

© 2011 S. Karger AG, Basel
ISSN 1662–6575
www.karger.com/cro

Possible Clinical Significance of Serum Soluble Interleukin-2 Receptor Level in Primary Bone Lymphoma: Two Case Reports

Hiroki Yabe[a] Hironori Ueno[b] Kensuke Ochi[c]
Hideo Morioka[d] Hiroo Yabe[d] Chihiro Terai[a]

[a]Division of Rheumatology, Jichi Medical University Saitama Medical Center, Saitama, [b]Department of Internal Medicine, National Hospital Organization Tokyo Medical Center, Tokyo, [c]Department of Orthopaedic Surgery, Kawasaki Municipal Kawasaki Hospital, Kawasaki, and [d]Department of Orthopaedic Surgery, Keio University School of Medicine, Tokyo, Japan

Key Words
Primary bone lymphoma · PBL · Soluble interleukin-2 receptor · sIL-2R · Tumor marker

Abstract
In two patients with primary bone lymphoma (PBL) treated in our clinic, serum levels of soluble interleukin-2 receptor (sIL-2R) reflected the clinical course. In both cases, sIL-2R levels were high before treatment and normalized with the therapeutic effects of chemotherapy, coinciding with the changes in lactate dehydrogenase levels and radiographic findings. Adding to the recently reported results of the diagnostic ability of sIL-2R in PBL, our case study highlights the clinical significance of serum sIL-2R levels as a tumor marker in PBL cases.

Introduction

Primary bone lymphoma (PBL) is an extremely rare malignant bone tumor. Patients with bone lesions usually visit rheumatology, orthopedic, or primary care clinics. Such clinicians should be reminded of the possibility of PBL when suspecting malignant bone tumors. Radiological diagnosis of PBL is often difficult because of its non-specific findings. Therefore, laboratory findings that help differentiate PBL from other primary bone tumors can play an important role. Serum soluble interleukin-2 receptor (sIL-2R) levels in patients with common primary malignant bone tumors except PBL were reported not to be significantly elevated compared to those in healthy subjects in previous reports [1, 2]. Recently, Akahane et al. [3] reported sIL-2R levels being significantly higher in PBL than in other malignant bone tumors and benign bone tumors/tumor-like lesions

Hiroki Yabe, MD
Division of Rheumatology, Jichi Medical University Saitama Medical Center
1-847 Amanuma-cho, Omiya-ku
Saitama City 330-8503 (Japan)
Tel. +81 48 647 2111, E-Mail yabehiroki@nyc.odn.ne.jp

and commented that the sIL-2R level is a valuable marker for diagnosing PBL. However, we were not able to find reports discussing the changes in serum sIL-2R levels during the clinical course in PBL. In this report, we present two PBL cases who had high serum levels of sIL-2R on presentation and normalized serum levels after the treatments. We show the clinical course of the two PBL patients and discuss the possible clinical significance of sIL-2R levels in PBL.

Case Report

Case 1

In May 2007 a 52-year-old man visited the National Hospital Organization Tokyo Medical Center (NTMC) with left buttock pain which had lasted for 6 months. X-ray and computed tomography (CT) tests were performed. The radiograph showed osteosclerotic and osteolytic changes in the wing of the ileum and the acetabulum (fig. 1a). A pathological fracture was observed in the acetabular roof. On CT imaging, we found expanded soft tissue around the ileum (fig. 1b). Bone scintigraphy showed highly increased accumulation of 99mTc-HMDP in the left acetabulum and indicated sole bone lesion. A whole-body CT scan and gallium scan revealed no evidence of visceral or lymph node involvement. From these results, a solitary primary malignant bone tumor was suspected.

Case 2

In August 2006, a 67-year-old man with a 1-month history of right hip pain visited the NTMC due to difficulty in walking. The radiograph showed osteolytic change in the acetabulum (fig. 1c). CT imaging showed moth-eaten pattern of destruction of the anterior part of the acetabulum and expanded soft tissue (fig. 1d). A whole-body CT scan, and bone and gallium scans were carried out. The scans revealed a solitary bone lesion. Thus, primary bone tumor of the right acetabular roof was suspected.

In both cases, laboratory tests at hospitalization showed high levels of serum sIL-2R [case 1: 2,880 U/ml, case 2: 1,140 U/ml (reference value: 188–570 U/ml)] and slightly elevated levels of lactate dehydrogenase (LDH) [case 1: 263 U/l, case 2: 241 U/l (reference value: approx. 119–229 U/l)]. The open biopsies of the tumors demonstrated proliferation of abnormal lymphoid cells. Immunohistochemistry revealed positive staining for CD20 and leukocyte common antigen, and was negative for CD3. Thus, both cases were diagnosed as PBL (diffuse large B-cell lymphoma). According to the Ann Arbor staging system, both localized bone lesions were regarded as stage I. The chemotherapy [R-CHOP (rituximab, cyclophosphamide, doxorubicin, vincristine, prednisolone); case 1: 8 courses, case 2: 6 courses] was performed under the supervision of the hematology department.

In case 1, osteosclerotic changes increased and the pathological fracture line became unclear in radiographic images after the chemotherapy (fig. 2a). New bone formation and increased osteosclerosis around the acetabulum as well as intrapelvic migration of the femur head were recognized in case 2 (fig. 2b). In both cases, soft tissue mass around the affected bone lesions was obviously decreased after treatment, as seen on CT images (fig. 2c, d). These radiological findings indicated the regression of pelvic bone lesions after treatment. Serum sIL-2R levels and LDH levels were normalized in both cases (fig. 3a, b), and linked with radiological therapeutic response of the affected bones.

Discussion

PBL is an extremely rare bone tumor; its frequency is considered to be about 3–7% of all primary malignant bone tumors, approximately 3% of all extranodal lymphomas, and less than 1% of all malignant lymphomas [4–7]. According to WHO classification, PBL can be categorized into two groups as follows: group 1, lymphoma involving a single skeletal site, with or without regional lymph-node involvement, and group 2, lymphoma